



저작자표시 2.0 대한민국

이용자는 아래의 조건을 따르는 경우에 한하여 자유롭게

- 이 저작물을 복제, 배포, 전송, 전시, 공연 및 방송할 수 있습니다.
- 이차적 저작물을 작성할 수 있습니다.
- 이 저작물을 영리 목적으로 이용할 수 있습니다.

다음과 같은 조건을 따라야 합니다:



저작자표시. 귀하는 원저작자를 표시하여야 합니다.

- 귀하는, 이 저작물의 재이용이나 배포의 경우, 이 저작물에 적용된 이용허락조건을 명확하게 나타내어야 합니다.
- 저작권자로부터 별도의 허가를 받으면 이러한 조건들은 적용되지 않습니다.

저작권법에 따른 이용자의 권리는 위의 내용에 의하여 영향을 받지 않습니다.

이것은 [이용허락규약\(Legal Code\)](#)을 이해하기 쉽게 요약한 것입니다.

[Disclaimer](#) 

Master's Thesis
석사 학위논문

Development of Hybrid Microbial Fuel Cell
for Improved Power Generation
under Solar Irradiation

Hyeon-Woo Kim(김 현 우 金鉉祐)

Department of Energy Systems Engineering
에너지시스템공학전공

DGIST

2015

Master's Thesis
석사 학위논문

Development of Hybrid Microbial Fuel Cell
for Improved Power Generation
under Solar Irradiation

Hyeon-Woo Kim(김 현 우 金鉉祐)

Department of Energy Systems Engineering
에너지시스템공학전공

DGIST

2015

Development of Hybrid Microbial Fuel Cell for Improved Power Generation under Solar Irradiation

Advisor : Professor Su-II In
Co-advisor : Professor Marie Kim

by

Hyeon-Woo Kim
Department of Energy Systems Engineering
DGIST

A thesis submitted to the faculty of DGIST in partial fulfillment of the requirements for the degree of Master of Science in the Department of Energy Systems Engineering. The study was conducted in accordance with Code of Research Ethics¹

01. 09. 2015

Approved by

Professor Su-II In _____ (Signature)
(Advisor)

Professor Marie Kim _____ (Signature)
(Co-Advisor)

¹ Declaration of Ethical Conduct in Research: I, as a graduate student of DGIST, hereby declare that I have not committed any acts that may damage the credibility of my research. These include, but are not limited to: falsification, thesis written by someone else, distortion of research findings or plagiarism. I affirm that my thesis contains honest conclusions based on my own careful research under the guidance of my thesis advisor.

Development of Hybrid Microbial Fuel Cell for Improved Power Generation under Solar Irradiation

Hyeon-Woo Kim

Accepted in partial fulfillment of the requirements
for the degree of Master of Science.

01. 09. 2015

Head of Committee _____(인)

Prof. Su-II In

Committee Member _____(인)

Prof. Marie Kim

Committee Member _____(인)

Ph.D Soo-Keun Lee

MS/ES
201324004

김 현 우. Hyeon-Woo Kim. Development of Hybrid Microbial Fuel Cell for Improved Power Generation under Solar Irradiation. Department of Energy Systems Engineering. 2015. 40 p. Advisors Prof. Su-Il In, Co-Advisors Prof. Marie Kim.

Abstract

Fossil fuels are running out because of human activities, and consumption of fossil fuels increases concentration of carbon dioxide that causes global warming. Therefore, developing a new renewable energy is needed. Microbial fuel cells (MFCs) are eco-friendly technology that can treat wastewater and generate bioelectricity at the same time. But there are some limitations such as low power output and expensive material cost. Thus, this study was conducted to overcome low efficiency of MFCs by developing a new solar hybrid system and current collector that can reduce internal resistance of MFCs.

First, suitable photoactive material must be used to harvest sunlight. In this study, N-doped TiO₂ nanotubes were used as photoanodes because of their photostability, high electron transfer ability and broad absorption range. Additional electrons are generated from photoanode by light irradiation and it increased power output around 34.9 % compared with a normal MFC reactor.

Second, the effect of current collectors was investigated. Current collector must have corrosion resistance in the aqueous solution. Therefore, titanium and stainless steel were used. Graphene oxide is coated on the current collector surface because of its excellent mobility of charge carriers, a large specific surface and good mechanical stability. The highest voltage was generated from the reactor which nanostructured stainless steel 304 mesh was used (452 mV).

Keywords: Microbial fuel cells, Photoactive material, Hybrid solar System, Anodization, Oxygen reduction reaction.

List of Contents

Abstract	i
List of Contents	ii
List of Figures	iv
List of Tables	v
List of Abbreviations	- 1 -
I. Introduction	- 2 -
1. Research Background.....	- 2 -
2. Electron Transfer Mechanism	- 3 -
3. References	- 5 -
II. Equipment	- 7 -
1. Field Emission Scanning Electron Microscope (FE-SEM).....	- 7 -
2. Potentiostat	- 8 -
3. X-ray Photoelectron Spectrometer (XPS).....	- 9 -
4. X-ray Diffractometer (XRD)	- 10 -
5. References	- 12 -
III. Investigation of N-doped Titanium Dioxide Nanotubes for The System of Hybrid Solar Microbial Fuel Cell	- 13 -
1. Introduction	- 13 -
2. Experimental Section	- 14 -
2.1 Materials	- 14 -
2.2 MFC set-up	- 15 -
2.3 Inoculum, substrate and medium.....	- 16 -
2.4 Photoanode preparation	- 16 -
2.5 Operating procedures.....	- 16 -
2.6 Preparation of SEM samples	- 17 -
2.7 Analysis	- 17 -
3. Results and Discussion.....	- 18 -
3.1 FE-SEM Analysis of Photoanode and Microorganisms on the Anode Surface	- 18 -

3.2	XRD patterns of photoanode.....	- 19 -
3.3	XPS analysis of photoanode.....	- 20 -
3.4	Photocurrent measurement of photoanode	- 22 -
3.5	Polarization and Power density curves of SMFC	- 22 -
4.	Conclusions	- 23 -
5.	References	- 25 -
IV.	Investigation of Current Collectors with Graphene Oxide Coating for Enhance Microbial Fuel Cells Performance	- 27 -
1.	Introduction	- 27 -
2.	Experimental Section	- 28 -
2.1	Materials	- 28 -
2.2	Electrical anodization of titanium mesh and stainless steel 304 mesh current collectors	- 28 -
2.3	Preparation of graphene oxide coated current collectors.....	- 28 -
2.4	Inoculum, substrate and medium.....	- 29 -
2.5	MFC set-up	- 29 -
2.6	Analysis	- 29 -
3.	Results and Discussion.....	- 29 -
3.1	SEM images of normal and graphene oxide coated current collectors.....	- 29 -
3.2	Voltage generation patterns of various microbial fuel cells.....	- 31 -
4.	Conclusions	- 32 -
5.	References	- 33 -
V.	Conclusions.....	- 35 -

List of Figures

Figure 1. Electron transfer mechanisms from microorganisms to electrode by (A) cell membrane, (B) soluble mediator and (C) conductive nanowires.	- 4 -
Figure 2. Schematic diagram of (A) SEM operation and (B) electron scattering by an electron beam.....	- 7 -
Figure 3. Schematic illustrations of (A) X-ray photoelectron spectrometer working principle and (B) photoelectron generation process.	- 9 -
Figure 4. Schematic diagram of (A) X-ray diffractometer and (B) Bragg's law.....	- 11 -
Figure 5. Schematic diagram of single chamber microbial fuel cell.....	- 15 -
Figure 6. Schematic diagram of SMFC system.	- 16 -
Figure 7. SEM images of (A) photoanode surface, (B) cross-section view of photoanode, (C), (D) normal carbon felt anode, and (E), (F) microorganisms attached to carbon felt anode and pilus-like structures (circle).	- 18 -
Figure 8. XRD patterns of photoanode before (black) and after (red) annealing.....	- 20 -
Figure 9. (A) survey spectra of photoanode, (B) N 1s spectra of photoanode, (C) C 1s spectra of photoanode, (D) Ti 2p spectra of photoanode and (E) O 1s spectra of photoanode.	- 21 -
Figure 10. Photocurrent density in glucose medium electrolyte and chopped current-time curve of photoanode (small box) with a three electrode configuration under 100 W Xe lamp illumination. The applied bias is 0 V vs. Ag/AgCl for chopped-time curve.	- 22 -
Figure 11. Polarization curve of SMFC (SMFC-V) and NMFC (NMFC-V). Power density curves of SMFC (SMFC-PD) and NMFC (NMFC-PD). Power densities and current density are normalized by the projected surface of the cathode electrode (7 cm ²).	- 23 -
Figure 12. Various current collectors before and after graphene oxide coating (A) Ti-wire, (B) G-Ti-wire, (C) Ti-mesh, (D) G-Ti-mesh, (E) AA-Ti-mesh, (F) G-AA-Ti-mesh, (G) SUS304-mesh, (H) G-SUS304-mesh, (I) A-SUS304-mesh and (J) G-A-SUS304-mesh.....	- 30 -
Figure 13. Voltage generation patterns of the MFCs with the various current collectors. (A) Ti-wire and G-Ti-wire, (B) Ti-mesh and G-Ti-mesh, (C) AA-Ti-mesh and G-AA-Ti-mesh, (D) SUS304-mesh and G-SUS304-mesh and (E) A-SUS304-mesh and G-A-SUS304-mesh.	- 31 -

List of Tables

Table 1. The list of reagents for vitamin stock solution - 14 -

Table 2. The list of reagents for mineral stock solution - 15 -

List of Abbreviations

MFC	Microbial Fuel Cell
MFCs	Microbial Fuel Cells
FE-SEM	Field Emission Scanning Electron Microscope
CP	Chronopotentiometry
LSV	Linear Sweep Voltammetry
XPS	X-ray Photoelectron Spectrometer
XRD	X-ray Diffractometer
ORR	Oxygen Reduction Reaction
SMFC	Hybrid Solar Microbial Fuel Cell
NMFC	Normal Microbial Fuel Cell
Ti-wire	Titanium Wire
G-Ti-wire	Graphene Coated Titanium Wire
Ti-mesh	Titanium Mesh
G-Ti-mesh	Graphene Coated Titanium Mesh
AA-Ti-mesh	Anodized & Annealed Titanium Mesh
G-AA-Ti-mesh	Graphene Coated, Anodized & Annealed Titanium Mesh
SUS304-mesh	Stainless Steel 304 Mesh
G-SUS304-mesh	Graphene Coated Stainless Steel 304 Mesh
A-SUS304-mesh	Anodized Stainless Steel 304 Mesh
G-A-SUS304-mesh	Graphene Coated, Anodized Stainless Steel 304 Mesh

I. Introduction

1. Research Background

The world's population has increased steadily. This population will need energy and at the same time, it will release huge wastes such as carbon dioxide that causes global warming and also contaminates water. This problem should be solved by developing renewable energy technology. Microbial fuel cells (MFCs) have received lots of attention.

MFCs generate electricity by using microorganisms as a biocatalyst in the anode side. The chemical energy stored in organic materials is converted into electrical energy by microorganisms. Electrochemically active microorganisms can generate and transfer electrons to an anode. These electrons flow to the external circuit. The external circuit consists of current collector and a resistor. In most MFCs, the electrons that reach the cathode combine with protons. These protons diffused from the anode through electrolyte and water is formed as a final product with oxygen provided from air.¹⁻³

MFCs operated with mixed cultures showed considerably greater power densities than those with pure cultures.⁴ Bacterial community analysis exist in MFCs publicized a great diversity in composition.⁵⁻⁷ MFCs have some advantages compared with inorganic fuel cells. They are very environmentally friendly, because electricity generated from the decomposition of wastes by microorganisms. Inorganic fuel cells are limited to several candidates as fuels. Hydrogen, methanol and ethanol are used in inorganic fuel cells. On the other hand, since microorganisms can utilize any carbon bearing substance, organic wastes can be used for MFCs. This technology is expected to apply to local wastewater treatment plant⁸ However, low efficiency and high cost are the bottlenecks for the application of MFCs.⁹ It was mostly caused by high internal resistance, slow oxygen reduction reaction (ORR) speed and cell configurations. There are many studies to increase power output of MFCs by reducing the internal resistance or enhancing electron transfer from microorganisms to electrode.¹⁰⁻¹²

The power density of MFCs has been improved dramatically, but further improvements are still required to use MFCs as promising bioelectricity production devices. The hybrid system with solar energy can be one

of the possible methods for increasing the efficiency of the microbial fuel cells. The solar light energy reaching earth in one hour is similar to the annual global consumption of energy. Therefore, harvesting the energy of solar light is a promising way to address the demand of energy supply.¹³ Solar light can be converted to electricity by using a semiconductor. Titanium dioxide (TiO₂) is mainly used because of its chemical inertness, non-toxicity and long-term stability against photo- and chemical-corrosion. However, the wide band gap energy (3.2 eV) limits the photocatalytic response of TiO₂. In order to improve the photo-response of TiO₂, a number of techniques have been developed. For example, photo-response of TiO₂ was increased by doping^{14, 15} and highly ordered TiO₂ nanotubes showed improved charge transfer.¹⁶

In this study, a hybrid MFC system with solar energy and MFC with various current collectors were examined. N-doped titanium dioxide nanotubes formed titanium foil (TNT-foil) was used to harvest sunlight because of its earth abundant, low cost and chemical stability.¹⁷ By irradiating solar light to the N-doped TiO₂ nanotubes, electrons can be generated and these electrons can be used for oxygen reduction reaction.

Secondly, loose contact between current collector and anode can be one of the reasons that causes unstable voltage generation. Therefore, to increase connection between current collector and the anode, the effect of current collector material, configuration and graphene oxide coating are investigated.

2. Electron Transfer Mechanism

There are three pathways of possible electron transfer from microorganisms to the anode. First, Figure 1 (A) displays that electrons are delivered by proteins located on the cell membrane upon direct contact with the anode surface.¹⁸ Membrane-associated electron transfer takes place through compounds that belong to the respiratory chain. *Geobacter metallireducens*¹⁹, *Aeromonas hydrophila*²⁰ and *Rhodospirillum rubrum*²¹ are using this pathway. Second, soluble mediators produced by bacteria can transfer electrons to electrode as shown in Figure 1 (B).²² In this case, electron transfer occurs in two ways i) through the production of reversibly reducible organic compounds such as pyocyanin and ii) through the generation of oxidizable metabolites such as H₂ and H₂S. *Shewanella putrefaciens* and *Pseudomonas aeruginosa* are using the mediators.²³⁻²⁵ These microbial mediators influence the performance of MFCs by increasing electron transfer efficiency. Electrons also can be transferred via microbial nanowires, which have a high electrical conductivity (Figure 1 (C)).²⁶ The electric conductivity of nanowires was investigated using *Geobacter*

species.²⁷

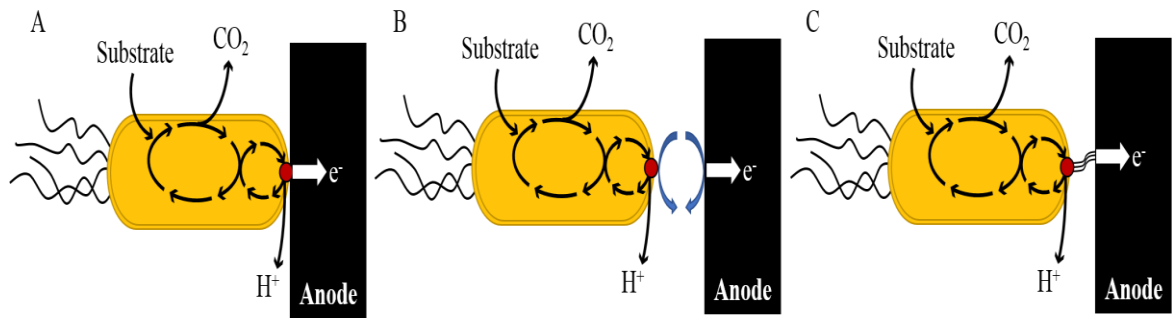


Figure 1. Electron transfer mechanisms from microorganisms to electrode by (A) cell membrane, (B) soluble mediator and (C) conductive nanowires.²⁸

3. References

1. Bond, D. R.; Holmes, D. E.; Tender, L. M.; Lovley, D. R., Electrode-reducing microorganisms that harvest energy from marine sediments. *Science* **2002**, 295 (5554), 483-485.
2. Chang, I. S.; Kim, B. H.; Kim, H. J.; Park, D. H.; Shin, P. K., Mediator-less biofuel cell. Google Patents: 1999.
3. Min, B.; Logan, B. E., Continuous electricity generation from domestic wastewater and organic substrates in a flat plate microbial fuel cell. *Environmental science & technology* **2004**, 38 (21), 5809-5814.
4. Rabaey, K.; Boon, N.; Höfte, M.; Verstraete, W., Microbial phenazine production enhances electron transfer in biofuel cells. *Environmental science & technology* **2005**, 39 (9), 3401-3408.
5. Aelterman, P.; Rabaey, K.; Pham, H. T.; Boon, N.; Verstraete, W., Continuous electricity generation at high voltages and currents using stacked microbial fuel cells. *Environmental science & technology* **2006**, 40 (10), 3388-3394.
6. Logan, B. E.; Murano, C.; Scott, K.; Gray, N. D.; Head, I. M., Electricity generation from cysteine in a microbial fuel cell. *Water Research* **2005**, 39 (5), 942-952.
7. Phung, N. T.; Lee, J.; Kang, K. H.; Chang, I. S.; Gadd, G. M.; Kim, B. H., Analysis of microbial diversity in oligotrophic microbial fuel cells using 16S rDNA sequences. *FEMS microbiology letters* **2004**, 233 (1), 77-82.
8. Logan, B. E.; Regan, J. M., Electricity-producing bacterial communities in microbial fuel cells. *TRENDS in Microbiology* **2006**, 14 (12), 512-518.
9. Du, Z.; Li, H.; Gu, T., A state of the art review on microbial fuel cells: a promising technology for wastewater treatment and bioenergy. *Biotechnology advances* **2007**, 25 (5), 464-482.
10. Fan, Y.; Hu, H.; Liu, H., Enhanced Coulombic efficiency and power density of air-cathode microbial fuel cells with an improved cell configuration. *Journal of Power Sources* **2007**, 171 (2), 348-354.
11. Rismani-Yazdi, H.; Carver, S. M.; Christy, A. D.; Tuovinen, O. H., Cathodic limitations in microbial fuel cells: an overview. *Journal of Power Sources* **2008**, 180 (2), 683-694.
12. Yong, X.-Y.; Shi, D.-Y.; Chen, Y.-L.; Jiao, F.; Lin, X.; Zhou, J.; Wang, S.-Y.; Yong, Y.-C.; Sun, Y.-M.; OuYang, P.-K., Enhancement of bioelectricity generation by manipulation of the electron shuttles synthesis pathway in microbial fuel cells. *Bioresource technology* **2014**, 152, 220-224.
13. Lewis, N. S.; Nocera, D. G., Powering the planet: Chemical challenges in solar energy utilization. *Proceedings of the National Academy of Sciences* **2006**, 103 (43), 15729-15735.
14. Qiu, X.; Burda, C., Chemically synthesized nitrogen-doped metal oxide nanoparticles. *Chemical Physics* **2007**, 339 (1), 1-10.
15. Asahi, R.; Morikawa, T.; Ohwaki, T.; Aoki, K.; Taga, Y., Visible-light photocatalysis in nitrogen-doped titanium oxides. *science* **2001**, 293 (5528), 269-271.
16. Mor, G. K.; Shankar, K.; Paulose, M.; Varghese, O. K.; Grimes, C. A., Use of highly-ordered TiO₂ nanotube arrays in dye-sensitized solar cells. *Nano letters* **2006**, 6 (2), 215-218.
17. Burda, C.; Lou, Y.; Chen, X.; Samia, A. C.; Stout, J.; Gole, J. L., Enhanced nitrogen doping in TiO₂ nanoparticles. *Nano letters* **2003**, 3 (8), 1049-1051.
18. Kostka, J. E.; Dalton, D. D.; Skelton, H.; Dollhopf, S.; Stucki, J. W., Growth of iron (III)-reducing bacteria

- on clay minerals as the sole electron acceptor and comparison of growth yields on a variety of oxidized iron forms. *Applied and Environmental Microbiology* **2002**, 68 (12), 6256-6262.
19. Rotaru, A.-E.; Shrestha, P. M.; Liu, F.; Markovaite, B.; Chen, S.; Nevin, K.; Lovley, D., Direct interspecies electron transfer between *Geobacter metallireducens* and *Methanosarcina barkeri*. *Applied and environmental microbiology* **2014**, AEM. 00895-14.
 20. Pham, C. A.; Jung, S. J.; Phung, N. T.; Lee, J.; Chang, I. S.; Kim, B. H.; Yi, H.; Chun, J., A novel electrochemically active and Fe (III)-reducing bacterium phylogenetically related to *Aeromonas hydrophila*, isolated from a microbial fuel cell. *FEMS Microbiology Letters* **2003**, 223 (1), 129-134.
 21. Chaudhuri, S. K.; Lovley, D. R., Electricity generation by direct oxidation of glucose in mediatorless microbial fuel cells. *Nature biotechnology* **2003**, 21 (10), 1229-1232.
 22. Rabaey, K.; Boon, N.; Siciliano, S. D.; Verhaege, M.; Verstraete, W., Biofuel cells select for microbial consortia that self-mediate electron transfer. *Applied and Environmental Microbiology* **2004**, 70 (9), 5373-5382.
 23. Angenent, L. T.; Karim, K.; Al-Dahhan, M. H.; Wrenn, B. A.; Domíguez-Espinosa, R., Production of bioenergy and biochemicals from industrial and agricultural wastewater. *TRENDS in Biotechnology* **2004**, 22 (9), 477-485.
 24. Hernandez, M.; Newman, D., Extracellular electron transfer. *Cellular and Molecular Life Sciences CMLS* **2001**, 58 (11), 1562-1571.
 25. Hernandez, M. E.; Kappler, A.; Newman, D. K., Phenazines and other redox-active antibiotics promote microbial mineral reduction. *Applied and environmental microbiology* **2004**, 70 (2), 921-928.
 26. Gorby, Y. A.; Yanina, S.; McLean, J. S.; Rosso, K. M.; Moyles, D.; Dohnalkova, A.; Beveridge, T. J.; Chang, I. S.; Kim, B. H.; Kim, K. S., Electrically conductive bacterial nanowires produced by *Shewanella oneidensis* strain MR-1 and other microorganisms. *Proceedings of the National Academy of Sciences* **2006**, 103 (30), 11358-11363.
 27. Reguera, G.; McCarthy, K. D.; Mehta, T.; Nicoll, J. S.; Tuominen, M. T.; Lovley, D. R., Extracellular electron transfer via microbial nanowires. *Nature* **2005**, 435 (7045), 1098-1101.
 28. Rinaldi, A.; Mecheri, B.; Garavaglia, V.; Licocchia, S.; Di Nardo, P.; Traversa, E., Engineering materials and biology to boost performance of microbial fuel cells: a critical review. *Energy & Environmental Science* **2008**, 1 (4), 417-429.

II. Equipment

1. Field Emission Scanning Electron Microscope (FE-SEM)

Field Emission Scanning Electron Microscopes (FE-SEM) use a focused electron beam and imaging one point at a time. The interaction of the electron beam with every point of the specimen surface is registered and then forming the entire image. Because of short wavelength of the electron beam, the magnification of the FE-SEM is much higher (thousands of times), than that of optical microscopes. Resolution of FE-SEM is about 1 nm to 20 nm.

Figure 2 (A) shows that Schematic diagram of FE-SEM operation. Electrons in the electron gun are emitted from the cathode and accelerated by the anode to the energy 1 ~ 50 keV. The electron beam is condensed by the condenser lenses (one or two). The electron beam, focused by the objective lens to very fine spot (1-5 nm), scans the sample surface in a raster pattern.

The kinds of the scattered electron generated by the collision with electron beam are shown in Figure 2 (B). Primary electrons interact with the atoms of the sample surface and the secondary electrons are emitted. By detecting these electrons, the image is produced. The backscattered electrons of the electron beam may also be detected. The backscattered electron image is used for contrasting the sample regions that have different chemical compositions.¹

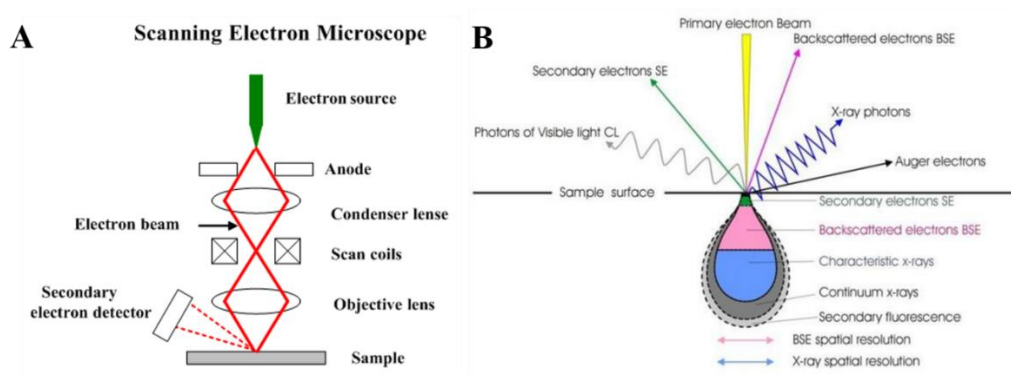


Figure 2. Schematic diagram of (A) SEM operation¹ and (B) electron scattering by an electron beam.²

2. Potentiostat

The galvanostatic mode uses three electrode configuration. A current is applied between auxiliary and working electrodes while the potential of the working electrode is monitored. In this case, redox (electron transfer) reaction must occur at the surface of the working electrode to support the applied current. Commonly it is used for constant current stripping potentiometry and constant current electrolysis, such as electrodeposition and battery studies.

Constant current techniques have one advantage that the ohmic drop due to solution resistance is also constant. On the other hand, in potentiostatic experiments such as the cyclic Voltammetry data correction is more complicated.

Chronopotentiometry (CP) is the most common constant current experiment that can obtain a polarization curve. Polarization curves were obtained from Bio-Logic Sas, VSP. An anode of microbial fuel cells was used as reference and counter electrode, and a cathode was used as working electrode. The current applied from 200 μA to 5000 μA with 200 μA intervals. Glucose medium ($5.6 \text{ mM} \cdot \text{L}^{-1}$) was used as electrolyte.³

Linear sweep voltammetry (LSV) is a voltammetric method. Potential between a working electrode and a reference electrode is swept linearly in time and the current at a working electrode is measured. It can identify unknown species and also can determine the concentration of solutions.⁴

In this study, the LSV is used to measure efficiency of photoactive material by measuring photocurrent. The sample was connected to the working electrode. Platinum wire and Ag/AgCl electrode were used as counter electrode and a reference electrode. The applied potential varied from -0.8 V to 0.8 V vs. Ag/AgCl electrode. Glucose medium ($5.6 \text{ mM} \cdot \text{L}^{-1}$) was used as electrolyte.

3. X-ray Photoelectron Spectrometer (XPS)

X-ray photoelectron spectroscopy is an analytical method that measures the valence states, elemental composition and the empirical formula of the elements that are present within a material. Figure 3 (A) shows the basic analytical process of XPS.

XPS spectra is measured by crushing a material with X-rays while simultaneously measuring the kinetic energy and the number of electrons that escape from the material. XPS is based on the photoelectric effect. Each atom on the surface has core electron with the characteristic binding energy that is conceptual, not strictly, equal to the ionization energy of that electron. When an X-ray beam directs to the sample surface, the energy of the X-ray photon is adsorbed completely by the core electron of an atom. If the photon energy, hn , is large enough, the core electron will then escape from the atom and emit out of the surface (Figure 3 B). The emitted electron with the kinetic energy of E_k is referred to as the photoelectron. The binding energy of the core electron is given by the Einstein relationship (eq. 1 and eq. 2).

$$h\nu = E_b + E_k + \phi \quad (1)$$

$$E_b = h\nu - E_k - \phi \quad (2)$$

Where $h\nu$ is the X-ray photon energy (for Al K α , $h\nu = 1486.6$ eV); E_k is the kinetic energy of photoelectron, which can be measured by the energy analyzer; and ϕ is the work function induced by the analyzer, about 4~5 eV. Since the work function, ϕ , can be compensated artificially, it is eliminated, giving the binding energy by changing (eq. 2) to (eq. 3).⁵

$$E_b = h\nu - E_k \quad (3)$$

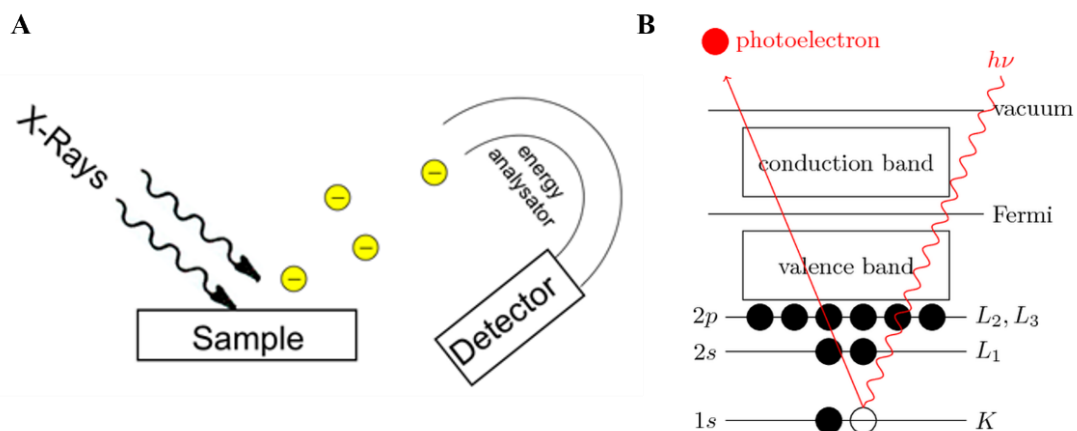


Figure 3. Schematic illustrations of (A) X-ray photoelectron spectrometer working principle⁶ and (B) photoelectron generation process.⁷

4. X-ray Diffractometer (XRD)

X-ray diffraction is a characterization analysis method that measures the crystallographic structure, lattice parameters, planar spacing, and crystallite size of materials. Figure 4 (A) shows the schematic diagram of X-ray diffractometer. It consists of X-ray source, sample stage and X-ray detector. X-ray generated from X-ray source and it hits an atom on the sample stage. Reflected X-ray is detected by X-ray detector. The specific mechanisms of XRD are described in Figure 4 (B). When an x-ray beam hits an atom, the electrons around the atom start to oscillate with the same frequency as the incoming beam. In almost all directions we will have destructive interference, that is, the combining waves are out of phase and there is no resultant energy leaving the solid sample. However the atoms in a crystal are arranged in a regular pattern, and in a very few directions we will have constructive interference. The waves will be in phase and there will be well defined x-ray beams leaving the sample at various directions. Hence, a diffracted beam may be described as a beam composed of a large number of scattered rays mutually reinforcing one another. This method is based on the principle of Bragg's law (eq. 4). The variable d is the distance between atomic layers in a crystal, and the variable lambda (λ) is the wavelength of the incident X-ray beam and n is an integer. Reflections occur from planes set at an angle θ with respect to the incident beam and generates a reflected beam at an angle $2 \cdot \theta$ from the incident beam. The possible d-spacing defined by the indices h, k, l are determined by the shape of the unit cell. Therefore the possible θ values where we can have reflections are determined by the unit cell dimensions (eq. 5). However, the intensities of the reflections are determined by the distribution of the electrons in the unit cell. The highest electron density is found around atoms. Therefore, the intensities depend on what kind of atoms we have and where in the unit cell they are located. Planes going through areas with high electron density will reflect strongly, planes with low electron density will give weak intensities.⁸

$$n * \lambda = 2d * \sin \theta \quad (4)$$

$$\sin \theta = \lambda / 2d \quad (5)$$

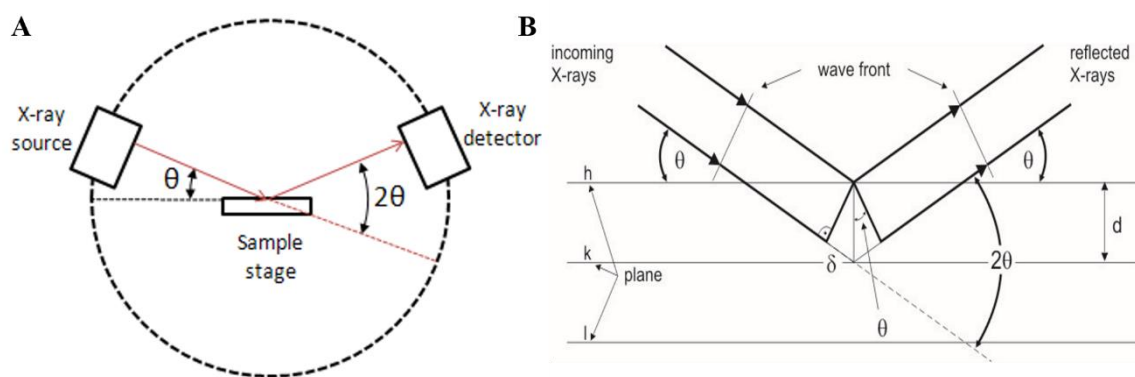


Figure 4. Schematic diagram of (A) X-ray diffractometer⁹ and (B) Bragg's law.¹⁰

5. References

1. http://www.substech.com/dokuwiki/doku.php?id=scanning_electron_microscope
2. <http://www.gla.ac.uk/schools/ges/research/researchfacilities/isaac/services/scanningelectronmicroscopy>
3. http://www.basinc.com/mans/EC_epsilon/Techniques/CPot/cp.html
4. http://en.wikipedia.org/wiki/Linear_sweep_voltammetry
5. <http://www2.cemr.wvu.edu/~wu/mae649/xps.pdf>
6. <http://www.e20.ph.tum.de/techniken/photoelectron-spectroscopy>
7. <http://www.texample.net/tikz/examples/principle-of-x-ray-photoelectron-spectroscopy-xps>
8. <http://old.vscht.cz/clab/RTG/dokumenty/thermo/xrd/Introduction%20to%20powder%20diffraction.pdf>
9. http://chemwiki.ucdavis.edu/Analytical_Chemistry/Instrumental_Analysis/Diffraction/Powder_X-ray_Diffraction
10. http://physik2.uni-goettingen.de/research/2_hofs/methods/XRD

III. Investigation of N-doped Titanium Dioxide Nanotubes for The System of Hybrid Solar Microbial Fuel Cell

1. Introduction

Microbial fuel cells (MFCs) are eco-friendly devices that treat wastewater. At the same time, these are producing a clean and renewable energy. However, oxygen reduction reaction (ORR) is one of the bottlenecks in MFC system. Because ORR, as a kinetically slow process, dominated the overall performance of MFC.¹ There are some attempts to combine MFCs with solar energy. For example, microbial electrolysis cell powered by a solar cell to generate H₂.² In this system, dye sensitized solar cell was used as an external power source. Also photosynthetic microorganisms were used to generate bioelectricity.^{3, 4} MFCs combined with photosynthetic microorganisms can produce electricity without the external input of exogenous organics or nutrients. Recently, H₂ generating device only using wastewater and sunlight was demonstrated.⁵ Up to our knowledge, there was no research attempts to make a single solar MFC device with a photoanode.

Solar energy is the radiant light and heat from the Sun. It is an important source of renewable energy. Development of solar energy technologies will have huge long-term benefits. For example, these technologies are inexhaustible, import-independent resource and reduce pollution.⁶ Therefore, a hybrid MFC system with solar energy can be one way to enhance power output of MFC.

In this study, hybrid solar MFC device (SMFC) was investigated. Additional electrons from the photoanode can be provided for ORR. To harvest solar light, N-doped titanium dioxide nanotubes formed on titanium foil were used as photoanode. N-doped TiO₂ nanotubes were made by anodization in the ethylene glycol electrolyte.^{7, 8} These structures offer a large internal surface area. Furthermore, the absorption and propagation can be influenced by controlling the architectural parameters such as wall thickness, nanotube pore size and length.⁹

The characteristics of photoanode were investigated by using X-ray diffractometer (XRD), X-ray photoelectron spectrometer (XPS) and field emission scanning electron microscope (FE-SEM). Electrochemical analysis of SMFC was conducted with potentiostat.

2. Experimental Section

2.1 Materials

Chemicals and reagents

Titanium mesh (Ti-mesh, 10 mesh, 0.5mm diameter) and titanium wire (Ti-wire, 1mm diameter) were used (Nilaco Corporation). All chemicals were purchased from the companies, Sigma, Appliedchem, Oxoid and used without further purification.

Vitamin stock solution

The reagents listed in Table 1 were dissolved in 800mL of distilled water. And then, the pH was adjusted to 7.0 with 1M-HCl and 1M-KOH with a pH meter (SCHOTT Instruments, Lab 850). The final volume was adjusted with distilled water (DI-water). The prepared vitamin stock solution was kept at 4°C to prevent decomposition of the temperature-sensitive reagents.

Table 1. The list of reagents for vitamin stock solution

Chemical	Amount (mg/L)
Biotin(d-biotin)	2
Folic acid	2
Pyridoxine HCl	10
Riboflavin	5
Thiamine HCl 1.0 H ₂ O	5
Nicotinic acid	5
d-pantothenic acid, hemicalcium salt	5
Vitamin B ₁₂	0.1
p-aminobenzoic acid	5
Lipoic acid	5

Mineral stock solution

The reagents listed in Table 2 were dissolved in 800mL of distilled water. The pH was adjusted to 7.0 with 1M-HCl and 1M-KOH with a pH meter (SCHOTT Instruments, Lab 850). The final volume adjusted with distilled water (DI-water) and The prepared vitamin stock solution was kept at 4°C to prevent decomposition of the temperature-sensitive reagents.

Table 2. The list of reagents for mineral stock solution

Chemical	Amount (/L)
Nitrilotriacetic acid	1.5 g
Magnesium sulfate heptahydrate	3 g
Manganese sulfate monohydrate	0.5 g
Sodium chloride	1 g
Ferrous sulfate heptahydrate	0.1 g
Calcium chloride dehydrate	0.1 g
Coblt chloride hexahydrate	0.1 g
Zinc chloride	0.13 g
Cupric sulfate pentahydrate	10 mg
Aluminum potassium disulfate dodecahydrate	10 mg
Boric acid	10 mg
Sodium molybdate dehydrate	25 mg
Nickel chloride hexahydrate	24 mg
Sodium tungstate	25 mg

2.2 MFC set-up

Figure 5 shows the single chamber MFC made with acryl. The working volume is 22 mL. Air-cathodes were prepared using wet-proofed carbon cloth (Fuel Cell Earth LLC, CCWP4030, projected surface area = 7 cm²) with diffusion layers and catalyst layer. Each cathode contains 0.5 mg Pt/cm² as described in the literature.¹⁰ Carbon felt (Samjungeng, Soft Felt, 2.0 cm x 2.1 cm x 1.0 cm) was used as the anode. Titanium mesh (Ti-mesh) was used as current collector. The cathode and anode were connected with titanium wire and an external resistor (1,000 Ω). The resistor was used as a load. The voltage generation was recorded by using a digital multimeter (Keithley, 2700).

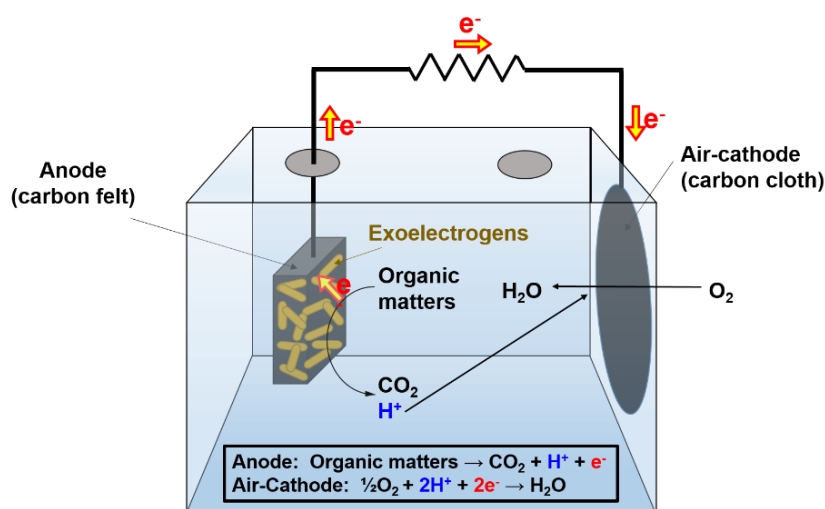


Figure 5. Schematic diagram of single chamber microbial fuel cell.

2.3 Inoculum, substrate and medium

The MFCs were inoculated with wastewater from Hyeonpung sewage treatment plant (Daegu, Korea). The medium contained glucose ($5.6 \text{ mM} \cdot \text{L}^{-1}$) as a substrate and a phosphate buffer solution containing : $17.8 \text{ mM} \cdot \text{L}^{-1} \text{ NaH}_2\text{PO}_4 \cdot \text{H}_2\text{O}$; $32.3 \text{ mM} \cdot \text{L}^{-1} \text{ Na}_2\text{HPO}_4$; $1.7 \text{ mM} \cdot \text{L}^{-1} \text{ KCl}$; $5.8 \text{ mM} \cdot \text{L}^{-1} \text{ NH}_4\text{Cl}$; trace vitamin and mineral stock solutions.¹¹ The initial pH was adjusted to 7.1. Reactors were kept at $30 \text{ }^\circ\text{C}$ in an incubator and were refilled when the voltage decreased below 20 mV.

2.4 Photoanode preparation

Titanium foil (Ti-foil, Nilaco Corporation, 453327) was cut to 6 cm x 4 cm size. And then, the surface of Ti-foil was cleaned by ultrasonic treatment in acetone, ethanol, and distilled water for 10 min each. One side of Ti-foil was covered with tape to prevent anodization. Ti-foil was connected to the anode of DC power supply (ODA Technologies Co., Ltd. OPE-1001S) and carbon paper (CNL Energy, 4.0 cm x 7.0 cm) was connected to the cathode as counter electrode. Prepared electrode was anodized in ethylene glycol electrolyte containing 0.5 wt% NH_4F and 2 vol% distilled water at 40 V for 30 min. After anodization, it was cleaned in ethanol with ultrasonic treatment for 2 min to remove debris. Subsequently, the anodized sample was annealed at $450 \text{ }^\circ\text{C}$ for 2 hours in air ($2 \text{ }^\circ\text{C}/\text{min}$).¹²

2.5 Operating procedures

The effect of SMFC system was tested. First, normal MFCs were operated with wastewater from Hyeonpung sewage treatment plant. These were operated more than 3 months for stabilization of voltage generation.

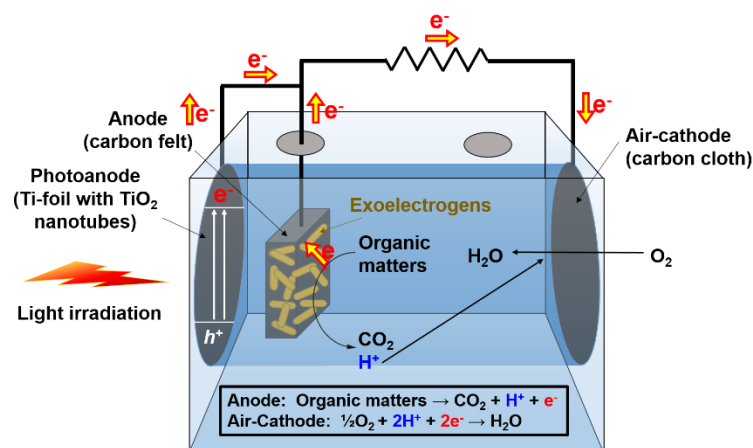


Figure 6. Schematic diagram of SMFC system.

After stabilization, one of normal MFCs was set with photoanode to make hybrid system. The SMFC system is shown in Figure 6. Additional electrons are generated from photoanode by light irradiation and these electrons can flow through the external circuit.

2.6 Preparation of SEM samples

Phosphate-buffered saline (PBS) containing $0.14 \text{ M} \cdot \text{L}^{-1}$ NaCl; $2.7 \text{ mM} \cdot \text{L}^{-1}$ KCl; $10 \text{ mM} \cdot \text{L}^{-1}$ Na_2HPO_4 , $1.8 \text{ mM} \cdot \text{L}^{-1}$ KH_2PO_4 was prepared. Glutaraldehyde was diluted from 25% to 2.5% by using PBS and the pH was adjusted to 7.0 by using 1 M NaOH solution. Anode of microbial fuel cells was cut (2 mm x 2 mm x 2 mm) and put into 2.5% glutaraldehyde solution for 1 hour to fix microorganisms. After one hour, solution was removed with micro pipette and 1 mL PBS was added. After 10 minutes samples were centrifuged at 8,000 rpm for 5 min. Glutaraldehyde was removed with same way. And then, dehydration step was followed by using 25, 50, 70, 85, 95 and 99.9% ethanol. After dehydration, the samples were dried at 55°C for 4 hours.

2.7 Analysis

Field emission scanning electron microscope (FE-SEM) was used to analyze the surface of anodized & annealed Ti-foil. The samples were coated by using a sputter coater (HITACHI MC1000, coating condition : $15 \mu\text{A}$ for 30 sec) to reduce charging effect.

X-ray diffraction patterns of photoanode were obtained by using Rigaku Mini-flex 600 X-ray Diffractometer. Scans were performed from 5° to 90° ($2.4^\circ/\text{min}$).

To investigate the chemical state of TiO_2 nanotubes on the surface of photoanode, X-ray Photoelectron Spectrometer (XPS) was employed.

Voltage generation was measured at 30 min intervals by using a multi-meter (Keithley, 2700) connected to a computer. Polarization curves were obtained by using a potentiostat (Bio-Logic Sas, VSP). The anode was used as working electrode and cathode was used as a counter and a reference electrode. The current was varied from $200 \mu\text{A}$ to $5,000 \mu\text{A}$ with $200 \mu\text{A}$ intervals. The current was applied for 1 min and the voltage output was recorded. The power generation of cells was calculated as $P=IV$. The power density (mW/m^2) and current density (mA/m^2) were normalized by projected cathode surface area (7 cm^2)

3. Results and Discussion

3.1 FE-SEM Analysis of Photoanode and Microorganisms on the Anode Surface

FE-SEM images of photoanode surface and microorganisms on the anode surface were obtained by using FE-SEM. The samples were fixed by using copper tape. The samples were coated with a platinum by using a sputter coater (HITACHI MC1000) at 15 μA for 30 sec. 3.0 kV and 10 μA were used during analysis.

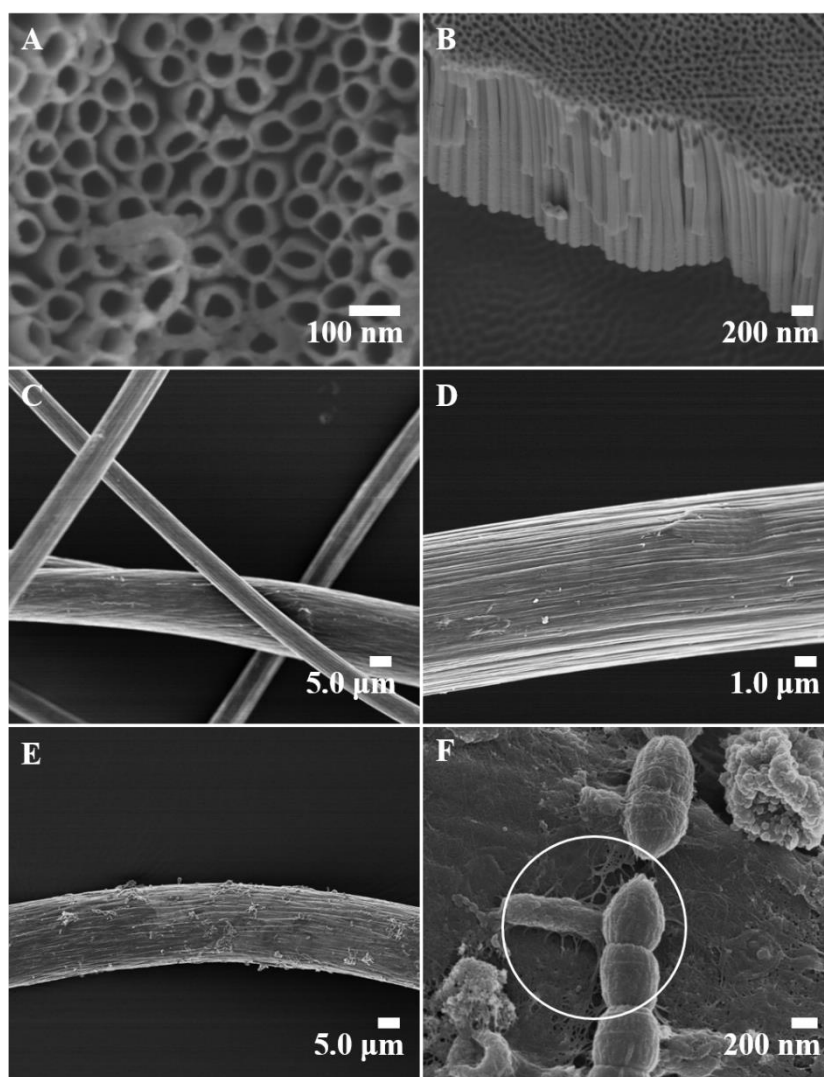


Figure 7. SEM images of (A) photoanode surface, (B) cross-section view of photoanode, (C), (D) normal carbon felt anode, and (E), (F) microorganisms attached to carbon felt anode and pilus-like structures (circle).

The FE-SEM images in Figure 7 reveal that the TiO_2 nanotubes on the surface of photoanode with an average diameter 119.1 nm and wall-thickness ≈ 39.6 nm (A), and cross-sectional view of TiO_2 nanotube

array with 1.42 μm in length (B). By irradiating light to the photoanode, additional electrons are generated. If the photon is absorbed, it has the possibility of exciting an electron from the valence band to the conduction band. A key factor of photon absorption is the energy of the photon. When the energy of photon is equal to or greater than the band gap of the N-doped anatase TiO_2 , the photon is absorbed by the N-doped anatase TiO_2 . The anatase TiO_2 1D structure has fast electron mobility. Therefore generated electrons can move rapidly. Further, electrons can flow through the external circuit of the SMFC. The normal carbon surface is shown in Figure 7 (C) and (D) as a control. After 5 months of operation, the morphology of the anode was examined by FE-SEM. Some microbial colonies were observed on the carbon felt anode (Figure 7 (E)). To confirm the species, additional analysis is needed such as 16s rRNA analysis.

The high-magnification image (Figure 7 (F)) reveals that bacterial cells are accumulated on the anode surface and cross-linked with each other to form a network by some pilus-like structures (circle) which are reported to play a key role in electron transfer and biofilm formation.¹³ To confirm whether it has electrical conductivity or not, additional analysis is needed. These bacterial nanowires affect to bacterial attachment. If it has electrical conductivity, electron transfer efficiency to anode will be enhanced. It makes nanoweb structure on the anode surface that makes microorganism attachment.

3.2 XRD patterns of photoanode

The XRD patterns of photoanode are provided in Figure 8. Before annealing of photoanode (Photoanode-B-A) showed the peaks of titanium metal. The peaks at 39.8° , 52.7° and 70.4° are attributed to (011), (012), and (110) planes of $\alpha\text{-Ti}$, respectively. After annealing of the photoanode (Photoanode-A-A) at 450°C for 2 hours, N-doped anatase TiO_2 nanotubes were formed on the surface of photoanode. The peaks at 25.0° , 37.5° , 47.8° and 53.7° are corresponding to (101), (004), (200) and (105) planes of anatase TiO_2 , respectively. The peak at 62.2° is corresponding to (002) plane of rutile TiO_2 . Therefore, it is anatase-rutile composite TiO_2 and it showed better photoactivity than pure anatase TiO_2 or rutile TiO_2 .¹⁴

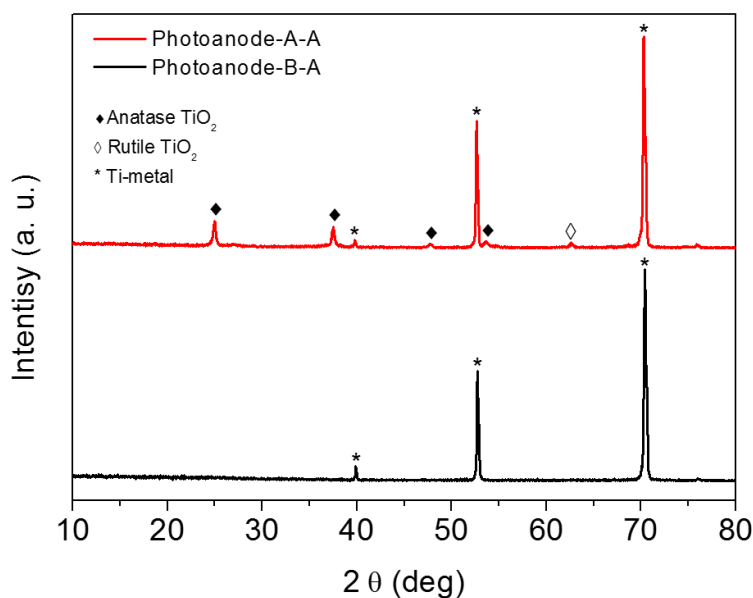


Figure 8. XRD patterns of photoanode before (black) and after (red) annealing.

3.3 XPS analysis of photoanode

The surface compositions of the photoanode were examined by XPS (Figure 9). The survey spectrum of photoanode (Figure 9 (A)) exhibits the presence of nitrogen ($1s = 399.8$ eV). N $1s$ core level from photoanode shows a single peak at 399.8 eV (Figure 9 (B)). Nitrogen peaks from TiN or chemisorbed nitrogen should appear less than 397.5 eV and NO or NO_2 type species appear above 400 eV.¹⁵⁻¹⁷ Few nitrogen in the TiO_2 lattice might reduce the electron density of nitrogen due to the high electronegativity of oxygen, hence a relatively higher binding energy has been observed, compared to TiN. The peaks at 284.2 eV and 284.5 eV (Figure 9 (C)) are corresponding to C $1s$ peaks were used as reference peak. Ti $2p_{3/2}$ core level appear at 458.4 eV for nitrogen-doped TiO_2 on the photoanode surface annealed at 450°C (Figure 9 (D)). On the other hand, Ti $2p_{3/2}$ core level of pure TiO_2 appeared at 459.3 eV.¹⁸ Lower binding energy of Ti $2p_{3/2}$ shows that the electronic interaction of Ti with anions is noticeably different than normal TiO_2 . It suggests that TiO_2 lattice is considerably modified due to N-substitution. The lower binding energy of Ti $2p$ in nitrogen-doped TiO_2 can be also explained on the basis of covalency between the Ti and nitrogen bond. The decrease of electronegativity of the anion causes the decrease of ionicity percentage.¹⁹ O $1s$ core level peak appears around 530 eV (Figure 9 (E)). A broadening on the higher binding energy side at 531.5 eV (indicated by an arrow) is clearly visible in the case of the N- TiO_2 sample.

It is clear from the above discussion that if the N atom is doped into the TiO₂ lattice, it is not likely to have significant interaction with nearby oxygen atoms too. However, an interstitial N-doping in the anatase lattice is likely to have some strong interaction with nearby oxygen and hence a change in effective charge on the nitrogen.

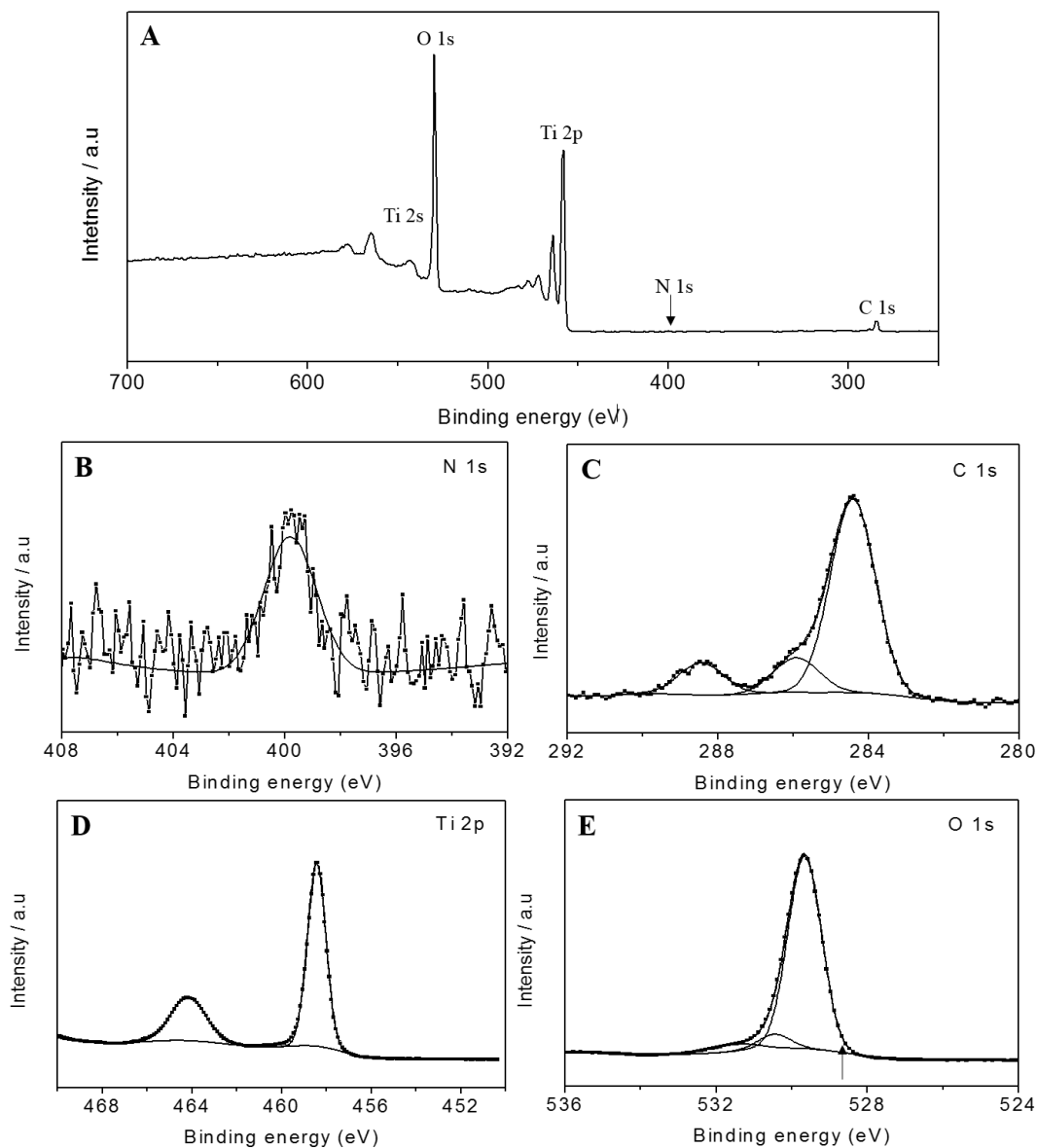


Figure 9. (A) survey spectra of photoanode, (B) N 1s spectra of photoanode, (C) C 1s spectra of photoanode, (D) Ti 2p spectra of photoanode and (E) O 1s spectra of photoanode.

Anatase TiO₂ can absorb only UV light, because it has wide bandgap energy (3.2 eV). However, N-doped anatase TiO₂ can absorb visible light because N-doping is narrowing the electronic band gap of TiO₂.²⁰ Therefore, N-doped TiO₂ can generate more electrons than pure TiO₂ under visible light.

3.4 Photocurrent measurement of photoanode

Figure 10 shows the photocurrent-voltage performance of photoanode sample. Photoanode was used as a working electrode and platinum wire was used as a counter electrode. The voltage applied from -0.8 V to 0.8 V vs. Ag/AgCl electrode. Photoanode was activated by 100W Xenon solar simulator (Oriel, LCS-100) with an AM1.5 filter. Glucose medium ($5.6 \text{ mM}\cdot\text{L}^{-1}$) was used as electrolyte. There was no current generation without light irradiation. On the other hand, the current was generated by light irradiation ($0.26 \text{ mA}/\text{cm}^2$ at 0 V vs. Ag/AgCl electrode). These electrons can flow through the external circuit and can be used for ORR. The photoelectrochemical response was measured light on/off illumination (small box) in order to confirm whether the photocurrent was specifically generated by only the absorbed photons without any dark current component. This showed a stable current generation during 2 min operation.

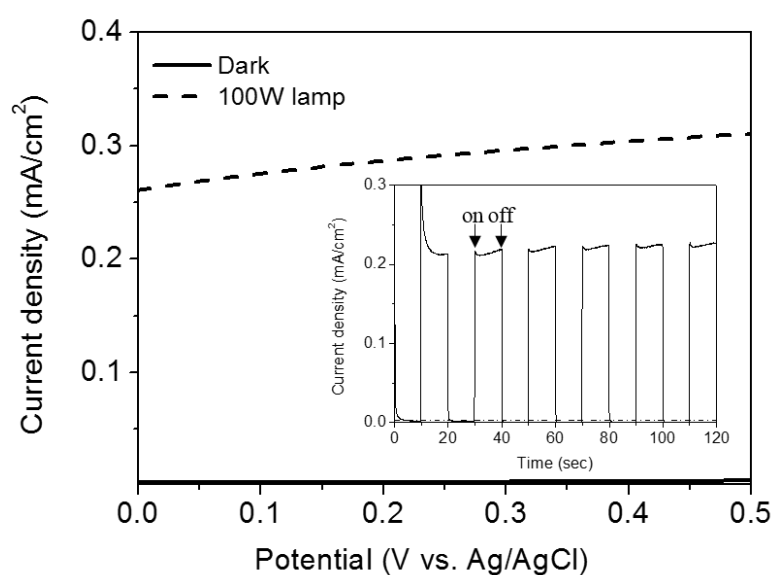
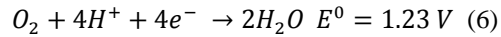


Figure 10. Photocurrent density in glucose medium electrolyte and chopped current-time curve of photoanode (small box) with a three electrode configuration under 100 W Xe lamp illumination. The applied bias is 0 V vs. Ag/AgCl for chopped-time curve.

3.5 Polarization and Power density curves of SMFC

The polarization properties of the SMFC are shown in Figure 11. The maximum current (I_{max}) from SMFC (SMFC-V) was slightly higher. It means that, electrons are generated by light irradiation and flow to cathode through the external circuit. At the photocurrent measurement, it was more than 0.26 mA. As

a result, higher current was generated. Four electrons are required to produce water (equation 6).²¹



Photoelectrons are helpful to form water as a final product by providing additional electrons. Furthermore, there are more chances to meet proton and oxygen. Thus, ORR speed can be increased. Because of the fast consumption of proton, there are proton concentration difference between the cathode side and the anode side. Therefore, protons are diffused to the cathode side faster than before. The internal resistances were calculated by using the slope. The internal resistances 179.8 Ω and 101.3 Ω are corresponding to NMFC and SMFC, respectively. Because of relatively small internal resistance of SMFC, the maximum power density obtained with SMFC (938.9 mW/m^2) at a current of 3.4 A. It was 34.9% higher than that obtained with normal MFC (NMFC, 696 mW/m^2).

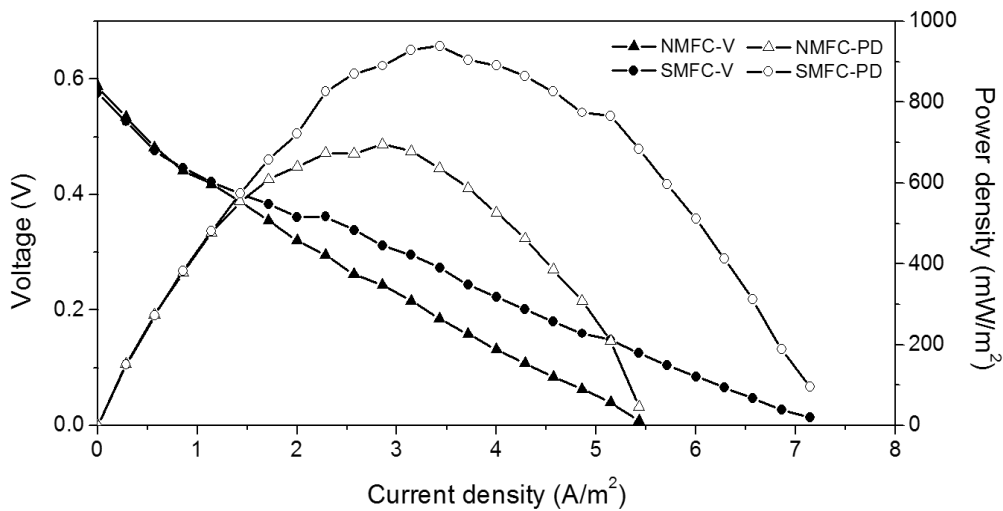


Figure 11. Polarization curve of SMFC (SMFC-V) and NMFC (NMFC-V). Power density curves of SMFC (SMFC-PD) and NMFC (NMFC-PD). Power densities and current density are normalized by the projected surface of the cathode electrode (7 cm^2).

4. Conclusions

Normally, power output of MFC is limited by slow ORR.²² To increase the performance of the MFC, hybrid solar microbial fuel cell system was developed using N-doped TiO_2 nanotubes. SEM images showed highly ordered N-doped TiO_2 nanotube structures on the photoanode. The formation of anatase TiO_2 crystal was confirmed by XRD analysis after annealing at 450 $^\circ\text{C}$ for 2 hours. Pure anatase TiO_2 cannot absorb

visible light. On the other hand, N-doping is narrowing the electrical band gap of TiO₂. Therefore, broader range of light can be absorbed. To confirm nitrogen doping, XPS patterns of photoanode were analyzed. The peak from nitrogen doped TiO₂ was observed at 399.8 eV. Photocurrent and chopped current-time curve showed photoelectrochemical property of photoanode. The photocurrent was 0.26 mA/cm² (0 V vs. Ag/AgCl). These electrons go to cathode through the external circuit. To form water as a final product, four electrons are needed. Therefore, the formation of water can be enhanced by photoelectrons. As a result, the highest power density is achieved from SMFC with light irradiation (938.9 mW/m²). This value was 34.9% higher than NMFC.

5. References

1. Liang, Y.; Li, Y.; Wang, H.; Zhou, J.; Wang, J.; Regier, T.; Dai, H., Co₃O₄ nanocrystals on graphene as a synergistic catalyst for oxygen reduction reaction. *Nature materials* **2011**, *10* (10), 780-786.
2. Chae, K.-J.; Choi, M.-J.; Kim, K.-Y.; Ajayi, F. F.; Chang, I.-S.; Kim, I. S., A solar-powered microbial electrolysis cell with a platinum catalyst-free cathode to produce hydrogen. *Environmental science & technology* **2009**, *43* (24), 9525-9530.
3. He, Z.; Kan, J.; Mansfeld, F.; Angenent, L. T.; Nealon, K. H., Self-Sustained Phototrophic Microbial Fuel Cells Based on the Synergistic Cooperation between Photosynthetic Microorganisms and Heterotrophic Bacteria. *Environmental Science & Technology* **2009**, *43* (5), 1648-1654.
4. McCormick, A. J.; Bombelli, P.; Scott, A. M.; Philips, A. J.; Smith, A. G.; Fisher, A. C.; Howe, C. J., Photosynthetic biofilms in pure culture harness solar energy in a mediatorless bio-photovoltaic cell (BPV) system. *Energy & Environmental Science* **2011**, *4* (11), 4699-4709.
5. Wang, H.; Qian, F.; Wang, G.; Jiao, Y.; He, Z.; Li, Y., Self-Biased Solar-Microbial Device for Sustainable Hydrogen Generation. *ACS nano* **2013**, *7* (10), 8728-8735.
6. IEA, *Solar Energy Perspectives*. OECD Publishing.
7. Paulose, M.; Shankar, K.; Yoriya, S.; Prakasam, H. E.; Varghese, O. K.; Mor, G. K.; Latempa, T. A.; Fitzgerald, A.; Grimes, C. A., Anodic growth of highly ordered TiO₂ nanotube arrays to 134 μm in length. *The Journal of Physical Chemistry B* **2006**, *110* (33), 16179-16184.
8. Shankar, K.; Mor, G. K.; Prakasam, H. E.; Yoriya, S.; Paulose, M.; Varghese, O. K.; Grimes, C. A., Highly-ordered TiO₂ nanotube arrays up to 220 μm in length: use in water photoelectrolysis and dye-sensitized solar cells. *Nanotechnology* **2007**, *18* (6), 065707.
9. Du, J.; Zhao, J. In *Effect of Electrolyte on the Morphology and Photocatalytic Properties of TiO₂ Nanotube Arrays*, Advanced Optoelectronics for Energy and Environment, Optical Society of America: 2013; p ASa3A. 47.
10. Cheng, S.; Liu, H.; Logan, B. E., Increased performance of single-chamber microbial fuel cells using an improved cathode structure. *Electrochemistry Communications* **2006**, *8* (3), 489-494.
11. Lovley, D. R.; Phillips, E. J., Novel mode of microbial energy metabolism: organic carbon oxidation coupled to dissimilatory reduction of iron or manganese. *Applied and environmental microbiology* **1988**, *54* (6), 1472-1480.
12. In, S.-I.; Vesborg, P. C.; Abrams, B. L.; Hou, Y.; Chorkendorff, I., A comparative study of two techniques for determining photocatalytic activity of nitrogen doped TiO₂ nanotubes under visible light irradiation: Photocatalytic reduction of dye and photocatalytic oxidation of organic molecules. *Journal of Photochemistry and Photobiology A: Chemistry* **2011**, *222* (1), 258-262.
13. Telford, J. L.; Barocchi, M. A.; Margarit, I.; Rappuoli, R.; Grandi, G., Pili in gram-positive pathogens. *Nature Reviews Microbiology* **2006**, *4* (7), 509-519.
14. Scanlon, D. O.; Dunnill, C. W.; Buckeridge, J.; Shevlin, S. A.; Logsdail, A. J.; Woodley, S. M.; Catlow, C. R. A.; Powell, M. J.; Palgrave, R. G.; Parkin, I. P., Band alignment of rutile and anatase TiO₂. *Nature materials* **2013**, *12* (9), 798-801.
15. György, E.; Perez del Pino, A.; Serra, P.; Morenza, J., Depth profiling characterisation of the surface layer

- obtained by pulsed Nd: YAG laser irradiation of titanium in nitrogen. *Surface and Coatings Technology* **2003**, 173 (2), 265-270.
16. Rainer, D.; Vesecky, S.; Koranne, M.; Oh, W.; Goodman, D., The CO+ NO Reaction over Pd: A Combined Study Using Single-Crystal, Planar-Model-Supported, and High-Surface-Area Pd/Al₂O₃ Catalysts. *Journal of Catalysis* **1997**, 167 (1), 234-241.
 17. Shinn, N.; Tsang, K. L., Strain-induced surface reactivity: Low temperature Cr/W (110) nitridation. *Journal of Vacuum Science & Technology A* **1991**, 9 (3), 1558-1562.
 18. Sathish, M.; Viswanathan, B.; Viswanath, R.; Gopinath, C. S., Synthesis, characterization, electronic structure, and photocatalytic activity of nitrogen-doped TiO₂ nanocatalyst. *Chemistry of materials* **2005**, 17 (25), 6349-6353.
 19. Viswanathan, B., Photocatalytic process-Selection criteria for the choice of materials. *Bull. Catal. Soc. Ind* **2003**, 2, 71.
 20. Tokudome, H.; Miyauchi, M., N-doped TiO₂ nanotube with visible light activity. *Chemistry Letters* **2004**, 33 (9), 1108-1109.
 21. Wendt, H.; Spinacé, E. V.; Oliveira Neto, A.; Linardi, M., Electrocatalysis and electrocatalysts for low temperature fuel cells: fundamentals, state of the art, research and development. *Química Nova* **2005**, 28, 1066-1075.
 22. Gil, G.-C.; Chang, I.-S.; Kim, B. H.; Kim, M.; Jang, J.-K.; Park, H. S.; Kim, H. J., Operational parameters affecting the performance of a mediator-less microbial fuel cell. *Biosensors and Bioelectronics* **2003**, 18 (4), 327-334.

IV. Investigation of Current Collectors with Graphene Oxide Coating for Enhance Microbial Fuel Cells Performance

1. Introduction

Water and energy are the essential elements to survive. Microbial fuel cell (MFC) is the key technology to clean water and generate energy. These technologies can be used in broad fields, such as wastewater treatment^{1,2}, biosensors^{3,4} and implantable medical devices.⁵ But, the low power output of MFCs is one of the main hurdles that limits practical application.⁶ Many attempts have been done to enhance performance of MFCs by changing the electrode material or configurations. Lately, there are a lot of tries to combine electrode materials and nanotechnologies.^{7,8} Nanoparticle-doped materials enhanced MFCs performances.^{9,10}

Another approach to enhance power output in MFCs is increasing contact area between electrode and current collector. The polarization losses of the cell and cell resistance were significantly reduced with the increase in the contact area of the current collector.¹¹

Recently, graphene has been considered as the intriguing material with great application potentials in various fields, such as solar cells¹², electrochemical super-capacitors¹³ and lithium ion batteries.¹⁴ The performance of MFCs can be increased by coating carbon base materials on the current collector.

In this study, graphene oxide (Graphene supermarket) was coated on the titanium and stainless steel 304 base current collectors because of its excellent mobility of charge carriers, a large specific surface and good mechanical stability.¹⁵ Titanium and stainless steel have long-term resistance to corrosion, electronic conductivity and biocompatibility.^{16,17} Graphene oxide coated current collectors have wrinkled and crumpled surface. This surface can offer increased contact area between current collector and the electrode. Therefore, graphene oxide modified current collectors have potential to increase the performance of MFC.

2. Experimental Section

2.1 Materials

Chemicals and reagents

Stainless steel 304 mesh (SUS304-mesh, 10 mesh, 0.5 mm diameter) was purchased from Dong Sung Wirenetting Co., Ltd. Titanium mesh (Ti-mesh, 10 mesh, 0.5mm diameter) and titanium wire (Ti-wire, 1mm diameter) were used that produce by Nilaco Corporation. All chemicals were purchased from the companies, Sigma, Appliedchem, Oxoid, Alfa aesar, Graphene supermarket and used without further purification.

2.2 Electrical anodization of titanium mesh and stainless steel 304 mesh current collectors

Titanium mesh (Ti-mesh, 10 mesh, 0.5 mm diameter) and stainless steel 304 mesh (SUS304-mesh, 10 mesh, 0.5 mm diameter) were cut (1.5 cm x 3.0 cm) and cleaned with acetone, ethanol, and distilled water for 10 min each by using ultrasonic treatment. Current collector was connected to the positive pole of DC power supply (ODA Technologies Co., Ltd. OPE-1001S) and carbon paper (1.5 cm x 4.0 cm) was connected to the negative pole of DC power supply as counter electrode.

Prepared samples were anodized at 40 V for 30 min in Ethylene glycol solution containing 0.3 wt% NH_4F and 2 vol% distilled water. After reaction, anodized Ti-mesh was smoothly cleaned by using distilled water and sonicated in ethanol for 2 min and it annealed at 450 °C for 1 hour (2 °C per min). Anodized SUS304-mesh was sonicated with acetone and ethanol for 10 min respectively.

2.3 Preparation of graphene oxide coated current collectors

Titanium wire (Ti-wire), titanium mesh (Ti-mesh), anodized Ti-mesh (A-Ti-mesh), stainless steel 304 mesh (SUS304-mesh) and anodized SUS304-mesh (A-SUS304-mesh) were prepared. Ultra high concentration graphene oxide aqueous solution (GRAPHENE SUPERMARKET, 6.2 g · L⁻¹) 5.6 mL and nafion solution (0.5 wt%) were mixed. Each electrode was deep into 0.5 mL prepared solution for 2 hours. And then, these are dried at 60 °C for 4 hours.

2.4 Inoculum, substrate and medium

The MFCs were inoculated with wastewater from Hyeonpung sewage treatment plant (Daegu, Korea). The medium contained glucose ($5.6 \text{ mM} \cdot \text{L}^{-1}$) as a substrate and a phosphate buffer solution containing : $17.8 \text{ mM} \cdot \text{L}^{-1} \text{ NaH}_2\text{PO}_4 \cdot \text{H}_2\text{O}$; $32.3 \text{ mM} \cdot \text{L}^{-1} \text{ Na}_2\text{HPO}_4$; $1.7 \text{ mM} \cdot \text{L}^{-1} \text{ KCl}$; $5.8 \text{ mM} \cdot \text{L}^{-1} \text{ NH}_4\text{Cl}$; trace vitamin and mineral stock solutions¹⁸. The initial pH was adjusted to 7.1. Reactors were kept at $30 \text{ }^\circ\text{C}$ in an incubator and were refilled when the voltage decreased below 20 mV.

2.5 MFC set-up

Single chamber MFCs were made using acryl with working volume 22 mL. Air-cathodes were prepared by using wet-proofed carbon cloth (Fuel Cell Earth LLC, CCWP4030, projected surface area = 7 cm^2) with diffusion layers and catalyst layer. Each cathode contains 0.5 mg Pt/cm^2 . Carbon felt (Samjungng, Soft Felt, $2.0 \text{ cm} \times 2.1 \text{ cm} \times 1.0 \text{ cm}$) was used as the anode. Ti-wire, Ti-mesh, AA-Ti-mesh, SUS304-mesh, A-SUS304-mesh, graphene oxide coated Ti-wire (G-Ti-wire), graphene oxide coated Ti-mesh (G-Ti-mesh), graphene oxide coated AA-Ti-mesh (G-AA-Ti-mesh), graphene oxide coated SUS304-mesh (G-SUS304-mesh) and graphene oxide coated A-SUS304-mesh (G-A-SUS304-mesh) were used as current collector. The cathode and anode were connected with titanium wire and an external resistor ($1,000 \text{ } \Omega$). The voltage generation was recorded by using a digital multimeter (Keithley, 2700).

2.6 Analysis

Field emission scanning electron microscope (FE-SEM) was used to analyze the surface of anodized & annealed Ti-foil. The samples were coated by using a sputter coater (HITACHI MC1000, coating condition : $15 \text{ } \mu\text{A}$ for 30 sec) to reduce charging effect.

Voltage generation was measured at 30 min intervals by using a multi-meter (Keithley, 2700) connected to a computer.

3. Results and Discussion

3.1 SEM images of normal and graphene oxide coated current collectors

Surface of various current collectors was investigated by using field emission scanning electron

spectroscopy (FE-SEM). Figure 12 (A), (C), (E), (G) and (I) reveal that the Ti-wire, Ti-mesh, AA-Ti-mesh, SUS304-mesh and A-SUS304-mesh, respectively. The surface of Ti-wire and SUS304-mesh looks flat compared with Ti-mesh, AA-Ti-mesh and A-SUS304-mesh. Thus, there is no enough surface area to contact with electrolyte and electrode that have accumulated electrons.

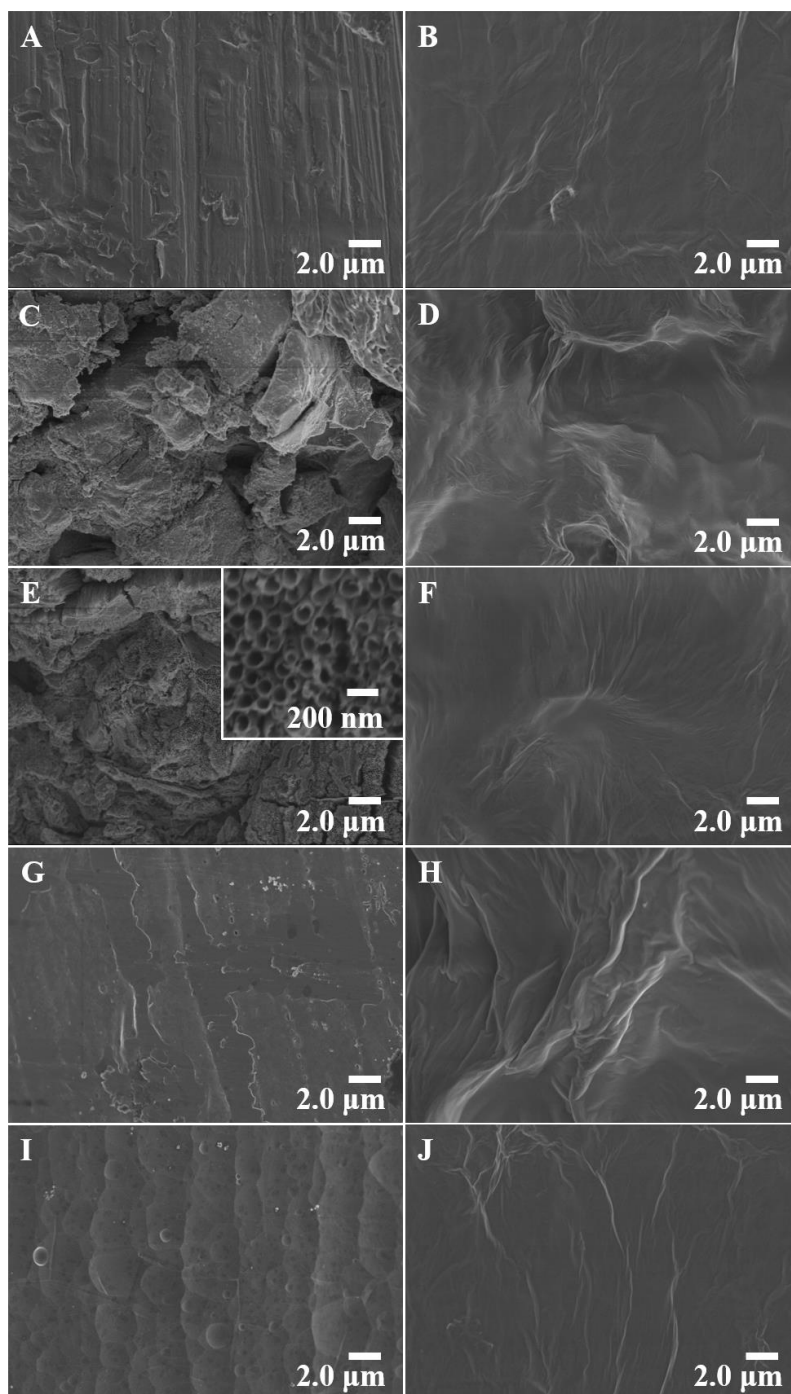


Figure 12. Various current collectors before and after graphene oxide coating (A) Ti-wire, (B) G-Ti-wire, (C) Ti-mesh, (D) G-Ti-mesh, (E) AA-Ti-mesh, (F) G-AA-Ti-mesh, (G) SUS304-mesh, (H) G-SUS304-mesh, (I) A-SUS304-mesh and (J) G-A-SUS304-mesh.

Figure 12 (B), (D), (F), (H) and (J) reveal that the graphene coated Ti-wire, Ti-mesh, AA-Ti-mesh, SUS304-mesh and A-SUS304-mesh, respectively. After graphene oxide coating, wrinkled and crumpled surface morphology was formed. This change has increased surface area that could enhance the interaction between current collector and electrode. In that case of Ti-mesh, A-Ti-mesh and A-SUS304-mesh (Figure 12 (C), (E) and (I), respectively), the structures were covered by graphene coating(Figure 12 (D), (F) and (J)). This change may reduce the benefits of the nano and porous structures.

3.2 Voltage generation patterns of various microbial fuel cells

Figure 13 shows voltage generations from (A) Ti-wire and G-Ti-wire current collector base MFCs, (B) Ti-mesh and G-Ti-mesh current collector base MFCs, (C) AA-Ti-mesh G-AA-Ti-mesh current collector

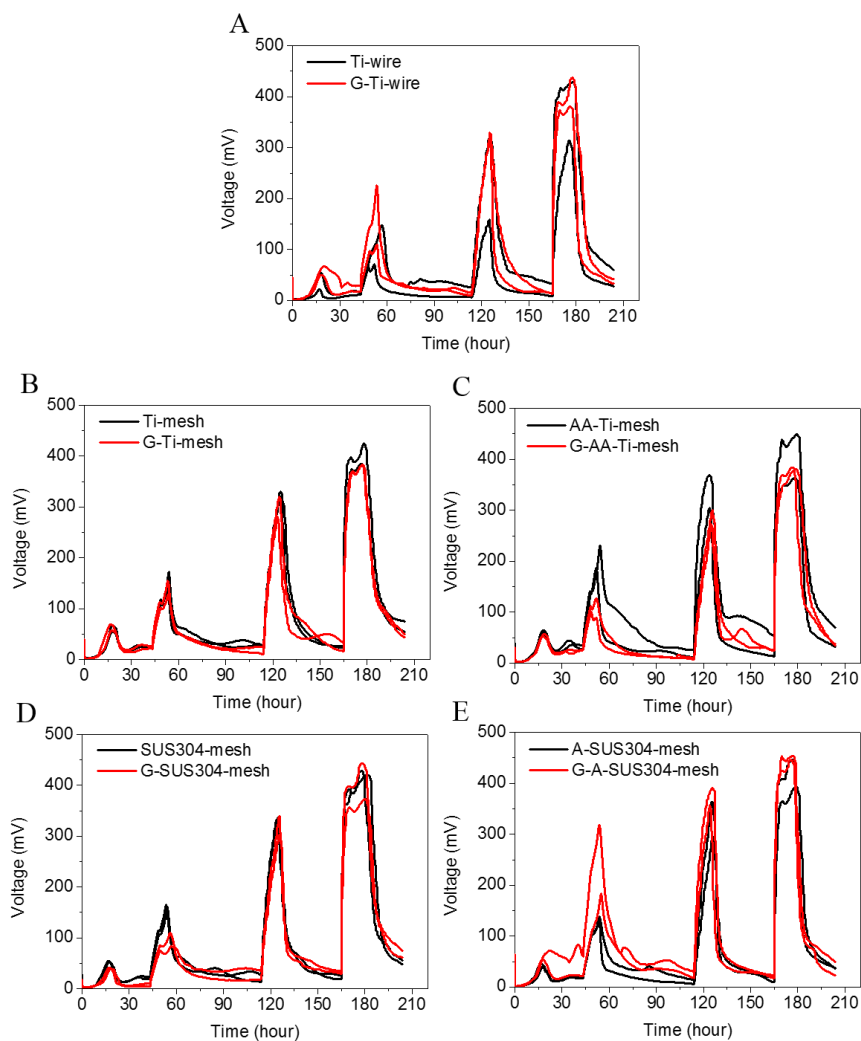


Figure 13. Voltage generation patterns of the MFCs with the various current collectors. (A) Ti-wire and G-Ti-wire, (B) Ti-mesh and G-Ti-mesh, (C) AA-Ti-mesh and G-AA-Ti-mesh, (D) SUS304-mesh and G-SUS304-mesh and (E) A-SUS304-mesh and G-A-SUS304-mesh.

base MFCs (D) SUS304-mesh and G-SUS304-mesh current collector base MFCs and (E) A-SUS304-mesh and G-A-SUS304-mesh current collector base MFCs.

After a 180 hour operation, the voltages generated from 313 mV to 452 mV. The highest voltage was generated from G-A-SUS304-mesh used MFC, but there was no significant difference between normal current collectors and graphene modified current collectors. It means that, there is no enhancement of interaction between electrodes and graphene modified current collectors.

4. Conclusions

In this study, the interaction between graphene coated current collector and electrodes was investigated. SEM images of graphene modified current collectors showed the formation of wrinkled and crumpled graphene layers. But, there was no enhancement of voltage generation after graphene coating. It seems to be a contact between the electrodes and modified current collectors unfulfilled in the microscopic region. For a more detailed study, the measurements of additional electrochemical characteristics such as polarization curve, cyclic voltammetry, EIS and power density are needed.

5. References

1. Rozendal, R. A.; Hamelers, H. V.; Rabaey, K.; Keller, J.; Buisman, C. J., Towards practical implementation of bioelectrochemical wastewater treatment. *Trends in biotechnology* **2008**, *26* (8), 450-459.
2. Sun, J.; Hu, Y.; Bi, Z.; Cao, Y., Improved performance of air-cathode single-chamber microbial fuel cell for wastewater treatment using microfiltration membranes and multiple sludge inoculation. *Journal of Power Sources* **2009**, *187* (2), 471-479.
3. Chang, I. S.; Jang, J. K.; Gil, G. C.; Kim, M.; Kim, H. J.; Cho, B. W.; Kim, B. H., Continuous determination of biochemical oxygen demand using microbial fuel cell type biosensor. *Biosensors and Bioelectronics* **2004**, *19* (6), 607-613.
4. Chang, I. S.; Moon, H.; Jang, J. K.; Kim, B. H., Improvement of a microbial fuel cell performance as a BOD sensor using respiratory inhibitors. *Biosensors and Bioelectronics* **2005**, *20* (9), 1856-1859.
5. Han, Y.; Yu, C.; Liu, H., A microbial fuel cell as power supply for implantable medical devices. *Biosensors and Bioelectronics* **2010**, *25* (9), 2156-2160.
6. Bullen, R. A.; Arnot, T.; Lakeman, J.; Walsh, F., Biofuel cells and their development. *Biosensors and Bioelectronics* **2006**, *21* (11), 2015-2045.
7. Ghasemi, M.; Daud, W. R. W.; Hassan, S. H.; Oh, S.-E.; Ismail, M.; Rahimnejad, M.; Jahim, J. M., Nano-structured carbon as electrode material in microbial fuel cells: a comprehensive review. *Journal of Alloys and Compounds* **2013**, *580*, 245-255.
8. Sarathi, V.; Nahm, K. S., Recent advances and challenges in the anode architecture and their modifications for the applications of microbial fuel cells. *Biosensors and Bioelectronics* **2013**, *43*, 461-475.
9. Gong, X.-B.; You, S.-J.; Wang, X.-H.; Zhang, J.-N.; Gan, Y.; Ren, N.-Q., A novel stainless steel mesh/cobalt oxide hybrid electrode for efficient catalysis of oxygen reduction in a microbial fuel cell. *Biosensors and Bioelectronics* **2014**, *55* (0), 237-241.
10. Yuan, Y.; Ahmed, J.; Zhou, L.; Zhao, B.; Kim, S., Carbon nanoparticles-assisted mediator-less microbial fuel cells using *Proteus vulgaris*. *Biosensors and Bioelectronics* **2011**, *27* (1), 106-112.
11. Jiang, S.; Love, J.; Apateanu, L., Effect of contact between electrode and current collector on the performance of solid oxide fuel cells. *Solid State Ionics* **2003**, *160* (1), 15-26.
12. Sheng, K.-x.; Xu, Y.-x.; Li, C.; Shi, G.-q., High-performance self-assembled graphene hydrogels prepared by chemical reduction of graphene oxide. *New Carbon Materials* **2011**, *26* (1), 9-15.
13. Vivekchand, S.; Rout, C. S.; Subrahmanyam, K.; Govindaraj, A.; Rao, C., Graphene-based electrochemical supercapacitors. *Journal of Chemical Sciences* **2008**, *120* (1), 9-13.
14. Yoo, E.; Kim, J.; Hosono, E.; Zhou, H.-s.; Kudo, T.; Honma, I., Large reversible Li storage of graphene nanosheet families for use in rechargeable lithium ion batteries. *Nano Letters* **2008**, *8* (8), 2277-2282.
15. Lee, C.; Wei, X.; Kysar, J. W.; Hone, J., Measurement of the elastic properties and intrinsic strength of monolayer graphene. *science* **2008**, *321* (5887), 385-388.
16. Pocaznoi, D.; Calmet, A.; Etcheverry, L.; Erable, B.; Bergel, A., Stainless steel is a promising electrode material for anodes of microbial fuel cells. *Energy & Environmental Science* **2012**, *5* (11), 9645-9652.
17. Yi, Q.; Huang, W.; Zhang, J.; Liu, X.; Li, L., A novel titanium-supported nickel electrocatalyst for cyclohexanol oxidation in alkaline solutions. *Journal of Electroanalytical Chemistry* **2007**, *610* (2), 163-

170.

18. Lovley, D. R.; Phillips, E. J., Novel mode of microbial energy metabolism: organic carbon oxidation coupled to dissimilatory reduction of iron or manganese. *Applied and environmental microbiology* **1988**, *54* (6), 1472-1480.

V. Conclusions

Microbial fuel cells (MFCs) are eco-friendly devices that generated electricity while treat wastewater. However, MFCs have bottlenecks such as low power output, high cost of materials that limit real application.

First, to increase efficiency of MFC, hybrid solar MFC (SMFC) system was investigated. Anodized & annealed Ti-foil used as photoanode to harvest sunlight. The images of highly ordered N-doped TiO₂ nanotube arrays were obtained by SEM. The XRD patterns showed the formation of anatase TiO₂ crystal after annealing at 450°C for 2 hours. Nitrogen doping was confirmed by XPS analysis. The peak at 399.8 eV is corresponding to N-doped TiO₂ XPS pattern. The fabrication of N-doped TiO₂ was easy and dependable, without using harsh condition. Furthermore, the resulting SMFC exhibited significantly improved performance (938.9 mW/m²) as compared with the normal MFC (696.0 mW/m²). The possible reason is that oxygen reduction reaction speed was increased by electrons generated from photoanode.

Second, the correlation between current collector materials and power output of MFCs were studied. Ti-wire, Ti-mesh, A-Ti-mesh, SUS304-mesh and A-SUS304-mesh were used as current collectors. After graphene coating on these current collectors, wrinkled and crumpled graphene layers were formed. However, there was no enhancement of voltage generation. It might come from slack contact between graphene modified current collectors and electrodes. For more specific information, additional electrochemical analysis is needed such as polarization curve, EIS, cyclic voltammetry and power density curve.

요 약 문

태양빛을 이용한 파워 생산 효율이 증가된

하이브리드 미생물 연료전지의 개발

세계적으로 인구의 수는 꾸준히 증가해 왔고, 이러한 인구수의 증가는 에너지를 필요로 할 것이며 동시에 지구온난화를 초래하는 이산화탄소와, 물을 오염시키는 물질들을 배출할 것이다. 이러한 문제는 새로운 신·재생 에너지 기술의 개발로 해결 해야 할 것이다. 미생물 연료전지 (Microbial fuel cells, MFCs)는 이러한 문제를 해결할 수 있는 기술 중 하나로 각광을 받고 있다.

미생물 연료전지란 anode 쪽에 붙어 자라는 미생물들의 촉매작용을 이용하여 유기물에 저장되어 있는 화학적 에너지를 전기에너지로 전환하는 장치이다. 전기화학적으로 활성이 있는 미생물들은 전자를 만들고 이를 anode로 전달할 수 있다. 이 전자는 current collector와 저항으로 이루어진 외부 회로를 통해 흐른다. 이 전자는 cathode 로 가며, 전해질로부터 확산되어 온 양성자, 외부에서 확산되어 온 산소와 결합하여 최종 생성물로 물을 만들게 된다. 이러한 반응을 산소환원 반응 이라고 한다.

미생물 연료전지의 경우 단일 균으로 작동하는 것 보다 혼합된 균을 사용했을 경우 비교적 많은 파워가 생성되었다. 미생물 연료전지 내에 있는 미생물 군집의 분석을 통해 다양한 조성이 있다는 것이 알려졌다. 일반 무기 연료전지와 비교해 봤을 때 미생물 연료전지는 몇 가지 장점이 있다. 우선, 전기가 미생물에 의한 오염물질의 분해로부터 발생하기 때문에 환경 친화적이다. 무기 연료전지의 경우는 오염물질을 분해하면서 전기를 발생시키지는 않는다. 또한 무기 연료전지의 경우 사용할 수 있는 연료가 수소 (H_2), 메탄올 (CH_3OH) 및 에탄올 (CH_2CH_3OH) 등으로 제한적이다. 하지만 미생물 연료전지의 경우, 탄소를 함유하고 있는 다양한 물질을 사용할 수 있다.

이 기술은 지역 하수처리장에 적용시켜서 사용할 수 있을 것으로 기대되었다. 하지만, 낮은 효

올과 비싼 재료 값은 미생물 연료전지를 이용하는데 있어 장애물로 작용한다. 미생물 연료전지의 또 다른 문제점은 current collector 와 anode 사이의 느슨한 접촉으로부터의 불안정한 전압 생성이다. 이러한 문제점은 높은 내부 저항과, 전지의 구성으로부터 온다. 따라서 내부 저항을 낮추거나, 미생물로부터 전극으로 전자를 전달하는 효율을 높임으로써 미생물 연료전지의 전력 생산을 높이려는 다양한 연구가 진행되었다.

미생물 연료전지의 전력 생산량은 급격하게 향상되어왔지만, 미생물 연료전지를 실질적인 바이오 전기 생산 장비로 이용하기 위해서는 추가적인 효율의 향상이 요구된다. 태양 에너지와 hybrid 된 시스템은 미생물 연료전지의 효율을 높이기 위한 여러 가지 방법들 중 한가지가 될 수 있다. 태양에너지는 고갈될 우려가 없는 에너지 자원이다. 한 시간 동안 지구에 도달하는 태양에너지의 양은 1 년간 소비되는 국제 에너지 소비량과 비슷하다. 따라서 태양빛으로부터 오는 에너지를 수집 하는 것은 에너지 공급 수요를 다룰 수 있는 유망한 방법이다.

미생물 연료전지를 태양에너지와 결합하려는 시도들이 있었다. 예를 들어, 미생물 전기 분해 셀로부터 수소를 생산하기 위해 태양전지로부터 전원을 공급받는 시스템이 연구되었다. 이 연구에서, 연료감응 태양전지가 외부 전원 공급원으로 사용되었다. 또한 미생물 연료전지의 경우 광합성미생물이 전기 생산을 위해 사용되었다. 이 경우 외부에서 유기물질이나 영양분을 넣어주지 않아도 전기 생산이 가능하다. 최근에는, 추가적인 외부 전원 공급원 없이 미생물 연료전지와 태양 에너지만을 이용하여 수소를 생산하는 장비가 개발되었다. 하지만 태양에너지를 이용하여 미생물 연료전지의 산소환원반응속도를 증가시키려는 시도는 없었다. 산소환원반응의 속도는 느리기 때문에 미생물 연료전지의 전체적인 효율을 감소시키는 여러 가지 요인들 중 한가지이다.

따라서 이 연구에서는 첫째로, 태양에너지를 수집할 수 있는 hybrid solar microbial fuel cell (SMFC) 시스템에 대해 조사되었다. 적당한 반도체 물질을 사용하면 태양 빛을 받음으로써 전자를 생성할 수 있고, 생성된 전자는 cathode 로 이동하여 산소환원반응에 참여할 수 있다. 따라서 반도체 물질로 매장량이 많고, 가격이 저렴하고, 화학적으로 안정한 특성 때문에, 티타늄 호일 표면에 질소가 도핑 된 TiO_2 나노튜브를 형성시켜 사용하였다.

우선 티타늄 호일 표면에 질소가 도핑 된 TiO_2 나노튜브를 만들기 위해 에틸렌글라이콜

(ethylene glycol) 용액 속에서 양극 산화시켰다. 에틸렌글라이콜 용액 속에는 0.5 중량%의 암모늄플로라이드 (NH_4F)와 2 볼륨%의 증류수가 포함되어 있으며, 상대전극으로는 카본페이퍼가 사용되었다. 양극산화는 40 V 에서 30 분간 이루어 졌으며, 반응 뒤 표면에 있는 불순물들을 제거하기 위해 증류수로 헹궈준 뒤에 에탄올에서 2 분간 초음파분쇄 하였다. 세척된 티타늄 호일 표면에 있는 비결정질의 질소가 도핑 된 TiO_2 나노튜브를 아나타제 구조로 만들어주기 위하여 가열로 안에서 450 °C 에서 2 시간동안 annealing 시켜줬다 (승온속도 : 2 °C/min).

XRD, XPS, FE-SEM 그리고 photocurrent 측정을 이용하여 이렇게 만들어진 photoanode 의 특성을 분석하였다.

FE-SEM 분석을 통해 질소가 도핑 된 TiO_2 나노튜브의 구조를 관찰하였다. 분석 결과 pore 의 평균 지름은 119.1 nm, 벽의 두께는 39.6 nm 그리고 나노튜브의 평균 길이는 1.42 μm 가 나왔다.

XRD 분석 에서는 annealing 하기 전과 후의 데이터를 비교하였다. Annealing 을 해주기 전에는 질소가 도핑 된 TiO_2 나노튜브가 비결정질을 띄기 때문에 티타늄 금속에 대한 XRD peak 만 볼 수 있었다. 하지만 2 시간동안 annealing 을 해준 경우에는 아나타제구조의 TiO_2 나노튜브 peak 을 확인할 수 있었다.

또한 질소가 도핑 된 것을 확인하기 위하여 XPS 분석을 하였다. 분석 결과 survey spectra 에서 O 1s, Ti 2p, N 1s 그리고 C 1s 에 대한 peak 들이 존재하는 것을 확인 할 수 있었다. N 1s peak 의 경우 399.8 eV 에서 peak 이 나왔다. TiN 결합이나 화학적으로 흡착된 N 1s peak 의 경우 397.5 eV 보다 낮은 곳에서 나오며, NO 또는 NO_2 결합에서 오는 N 1s peak 은 400 eV 보다 높은 곳에서 나온다. Ti 2p_{3/2} peak 의 경우 458.3 eV 에서 나왔는데 이는 일반적으로 459.3 eV 에서 나오는 TiO_2 의 Ti 2p_{3/2} peak 보다 낮은 곳에서 나왔다. 이러한 peak shift 현상은 음이온의 전기음성도 감소로 인해 이온 성 또한 감소했기 때문이다. O 1s core peak 의 경우 530 eV 에서 나왔는데, 531 eV 에서 peak 의 폭이 넓어지는 현상은 N- TiO_2 sample 에서 발견되는 현상이다. C 1s peak 의 경우 기준 peak 으로 사용되었다.

위에서 언급한 결과들에 의해 질소가 TiO_2 격자에 도핑이 되었다는 것을 알 수 있다. 질소를 TiO_2 에 도핑 할 경우 밴드 갭이 줄어들기 때문에 가시광선 영역의 빛을 흡수 할 수 있다. 따라서

일반 TiO_2 를 사용하는 것보다 더 많은 전자의 생성이 가능하게 된다.

마지막으로 photoanode 의 전기화학적 특성을 분석하기 위해 photocurrent 를 측정하였다. 전해질은 2 g/L 의 농도로 만들어진 glucose medium 을 이용하였으며, Ag/AgCl 전극을 기준전극으로, platinum wire 를 상대전극으로 사용하였다. 기준전극 대비 -0.8 V 부터 0.8 V 까지 측정하였고, 측정 결과 0 V 에서 0.26 mA 의 photocurrent 값을 보였다.

이렇게 준비된 photoanode 를 미생물 연료전지에 적용 시키기 위해 일반적인 미생물 연료전지를 3 개월 이상 작동시켰다. 미생물 연료전지의 전압 생성 패턴이 안정화 되고 난 후, photoanode 를 일반적인 단일 미생물 연료전지에 연결하였고, 전기화학적인 분석을 위해 I-V curve 와 powerdensity 를 측정하였다. Anode 는 기준전극 겸 상대전극으로 사용되었고, cathode 는 작업전극으로 사용되었다. 전류를 200 μA 씩 바꿔가면서 1 분동안 가해줬고 그때 나오는 전압 값을 기록하였다. 전류의 값이 0 이하로 떨어질 때까지 측정을 계속해줬다. 측정 결과로 얻은 I-V curve 를 통해 photoanode 에 빛을 조사해줬을 경우 더 회로에 더 많은 양의 전류가 흐른다는 것을 알 수 있었다. 이 추가적인 전류는 photoanode 에 빛을 조사함으로써 생성되는 전자로부터 기인한 것이며, 이 전자들은 cathode 쪽에서 산소환원반응에 참여할 수 있다. 따라서 산소환원반응의 속도를 증가시킬 수 있다. Power density 의 결과로부터 빛을 조사했을 경우 빛을 조사하지 않은 반응조에 비해 power density 가 34.9% 증가한 것을 확인할 수 있었다.

결론적으로 산소환원반응속도의 증가로 인한 미생물 연료전지의 효율 증가를 보기 위해 질소가 도핑 된 TiO_2 나노튜브가 photoanode 로 이용되었다. 이러한 질소가 도핑 된 TiO_2 나노튜브는 티타늄 호일을 에틸렌글라이콜 용액에서 양극산화를 통해 얻어졌으며 이러한 photoanode 의 특성은 FE-SEM, XRD, XPS 그리고 photocurrent 를 통하여 분석하였다. 분석 결과 질소가 도핑 된 TiO_2 나노튜브가 티타늄 호일 표면에 형성되었으며, Ag/AgCl 기준전극 대비 0 V 에서 0.26 mA 의 photocurrent 가 생성되었다. 이렇게 추가적으로 생성된 전자는 회로의 전류 값을 증가시켰으며 결론적으로 빛을 조사하지 않았을 때에 비해 34.9% 증가된 power density 값을 보였다.

둘째로, 미생물 연료전지의 또 다른 문제점 중 하나는 current collector 와 anode 사이의 느슨한 접촉이다. 따라서 current collector 의 종류, 구조 그리고 graphene oxide 를 코팅했을 경우 미

생물 연료전지에 어떤 영향을 미치는지에 대해 조사되었다. 사용된 current collector 의 종류는 Ti-wire, G-Ti-wire, Ti-mesh, G-Ti-mesh, AA-Ti-mesh, G-AA-Ti-mesh, SUS304-mesh, G-SUS304-mesh, A-SUS304-mesh, G-A-SUS304-mesh 로 총 10 가지였다.

우선 Ti-mesh 와 SUS304-mesh 에 나노 구조를 만들기 위해 에틸렌글라이콜 용액 속에서 양극 산화시켰다. 그 뒤 Ti-mesh 의 경우 표면의 불순물들을 제거하기 위해 증류수로 씻어준 뒤 에탄올 용액에서 2 분간 초음파분쇄 시켜줬다. 그리고 표면에 아나타제구조의 TiO₂ 나노튜브를 만들기 위해 450 °C 에서 1 시간동안 annealing 했다. 그리고 나서 graphene oxide 를 코팅하기 위해 Ti-wire, Ti-mesh, A-Ti-mesh, SUS304-mesh, A-SUS304-mesh 를 각각 0.5 mL 의 graphene oxide 용액에 2 시간동안 담궈두었다가 꺼내 60 °C 에서 건조시켰다.

FE-SEM 을 통해 준비된 current collector 들의 표면 구조를 관찰하였다. 관찰 결과 양극산화 후 annealing 한 Ti-mesh 의 경우 표면에 나노튜브들이 형성된 것을 확인할 수 있었고, 양극 산화된 SUS304-mesh 의 경우 표면에 나노 사이즈의 다공들이 형성된 것을 확인할 수 있었다. Current collector 에 graphene oxide 를 코팅한 경우 주름이 진 표면을 확인 할 수 있었다.

준비된 current collector 들을 이용하여 미생물 연료전지들을 셋업 한 뒤 멀티미터를 이용하여 반응조로부터 생성되는 전압 값을 기록하였다. 전압 값들을 비교 해본 결과 G-A-SUS304-mesh current collector 를 이용한 미생물 연료전지에서 가장 높은 전압이 생성되었다. 하지만 10 가지의 다른 current collector 들을 사용한 반응조에서 생성된 전압값에는 큰 차이가 없었다. 따라서 좀 더 정확한 분석을 위해서는 EIS, CV, I-V curve 및 power density 와 같은 추가적인 전기화학적 분석이 필요할 것으로 생각된다.

핵심어 : 미생물 연료전지, 광활성 물질, 광 하이브리드 시스템, 양극산화, 산소환원반응